Article

Cell Host & Microbe

Red Blood Cell Invasion by the Malaria Parasite Is Coordinated by the PfAP2-I Transcription Factor

Graphical Abstract

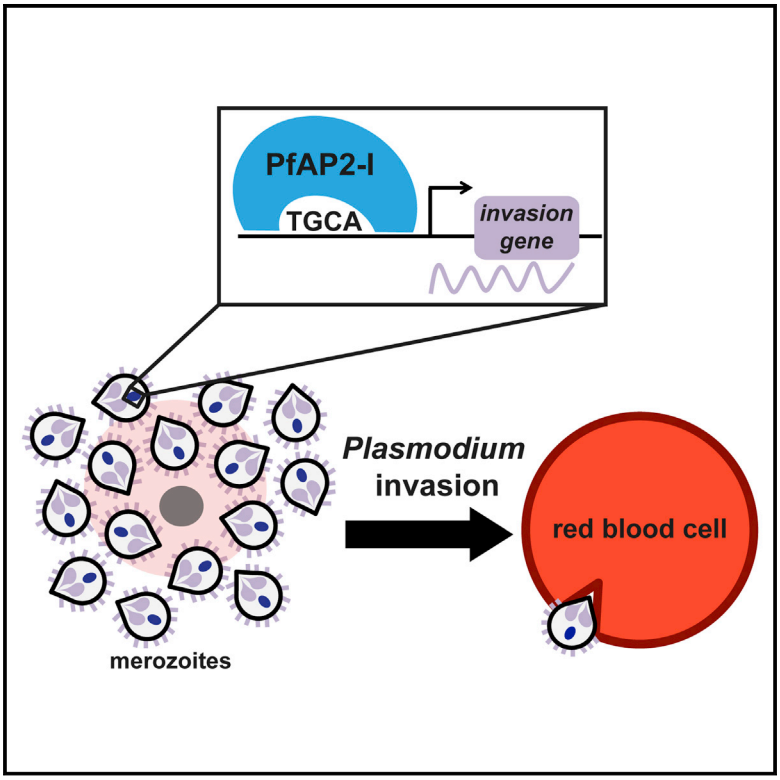

Authors

Joana Mendonca Santos, Gabrielle Josling, Philipp Ross, ..., Ariel Schieler, Ileana M. Cristea, Manuel Llinás

Correspondence

manuel@psu.edu

In Brief

Invasion of red blood cells is a highly regulated and essential process in the life cycle of the malaria parasite *Plasmodium falciparum*. Santos et al. identify a transcription factor (PfAP2-I) that regulates invasion genes during blood stage development and associates with *P. falciparum* bromodomain protein 1 (PfBDP1).

Highlights

- PfAP2-I binds a DNA motif enriched upstream of merozoite invasion genes
- PfAP2-I binding to the invasion DNA motif is necessary for target gene transcription
- Only the C-terminal AP2 domain of PfAP2-I is essential for asexual stage activity
- PfAP2-I and PfBDP1 co-IP and regulate transcription of many of the same genes

Santos et al., 2017, Cell Host & Microbe *21*, 731–741
June 14, 2017
http://dx.doi.org/10.1016/j.chom.2017.05.006

Cell Host & Microbe
Article

Red Blood Cell Invasion by the Malaria Parasite Is Coordinated by the PfAP2-I Transcription Factor

Joana Mendonca Santos,[1,2,3] Gabrielle Josling,[1,5] Philipp Ross,[1,5] Preeti Joshi,[2] Lindsey Orchard,[1] Tracey Campbell,[2,3] Ariel Schieler,[2,3] Ileana M. Cristea,[2] and Manuel Llinás[1,2,3,4,6,*]
[1]Department of Biochemistry and Molecular Biology and Huck Center for Malaria Research, Pennsylvania State University, State College, PA 16802, USA
[2]Department of Molecular Biology
[3]Lewis-Sigler Institute for Integrative Genomics
Princeton University, Princeton, NJ 08544, USA
[4]Department of Chemistry and Huck Center for Infectious Disease Dynamics, Pennsylvania State University, State College, PA 16802, USA
[5]These authors contributed equally
[6]Lead Contact
*Correspondence: manuel@psu.edu
http://dx.doi.org/10.1016/j.chom.2017.05.006

SUMMARY

Obligate intracellular parasites must efficiently invade host cells in order to mature and be transmitted. For the malaria parasite *Plasmodium falciparum*, invasion of host red blood cells (RBCs) is essential. Here we describe a parasite-specific transcription factor PfAP2-I, belonging to the Apicomplexan AP2 (ApiAP2) family, that is responsible for regulating the expression of genes involved in RBC invasion. Our genome-wide analysis by ChIP-seq shows that PfAP2-I interacts with a specific DNA motif in the promoters of target genes. Although PfAP2-I contains three AP2 DNA-binding domains, only one is required for binding of the target genes during blood stage development. Furthermore, we find that PfAP2-I associates with several chromatin-associated proteins, including the Plasmodium bromodomain protein PfBDP1 and that complex formation is associated with transcriptional regulation. As a key regulator of red blood cell invasion, PfAP2-I represents a potential new antimalarial therapeutic target.

INTRODUCTION

The phylum Apicomplexa consists of obligate intracellular eukaryotic parasites, including *Plasmodium falciparum*, the major causative agent of malaria. In the human host, *P. falciparum* merozoites invade red blood cells (RBCs), in which they grow and divide by schizogony during the 48 hr intraerythrocytic developmental cycle (IDC). Following replication, schizonts rupture and release 16–32 newly formed merozoites (Reilly et al., 2007), which egress from the RBC prepackaged with the proteins necessary for a new round of RBC invasion. Malaria symptoms, including fever and anemia, are correlated with the periodic and exponentially increasing waves of merozoite egress and invasion.

RBC invasion by the malaria parasite involves an orchestrated sequence of protein-protein interactions between the parasite and its host. Proteins mediating invasion decorate the merozoite surface or are stored at the apical end of the parasite in specialized secretory organelles named micronemes and rhoptries (Figure 1A) (Gao et al., 2013; Singh and Chitnis, 2012). Of the ten known merozoite surface proteins (PfMSP1–PfMSP10), PfMSP1 is the most abundant, with roles in merozoite egress (Das et al., 2015), budding (Combe et al., 2009), and likely the first steps of RBC attachment (Weiss et al., 2015). Stable adhesion of the parasite to RBCs is further mediated by proteins secreted from the rhoptry necks (the reticulocyte homologs, or Rhs) and proteins originating in the micronemes (the erythrocyte binding-like proteins, or EBLs) through specific interactions with host cell receptors (Tham et al., 2012). The rhoptry neck proteins (RONs), on the other hand, form a complex with the micronemal protein apical membrane antigen (PfAMA1) at the tight junction formed at the site of parasite attachment to the RBC membrane (reviewed in Proellocks et al., 2010). Merozoite invasion is an active process propelled by the glideosome, which is anchored between the plasma membrane and the inner membrane complex (IMC). This is a large molecular machine composed of a myosin motor (PfMyoA), a myosin light chain (myosin A tail domain-interacting protein, or PfMTIP), and several glideosome-associated proteins (GAPs) (Frénal et al., 2010). The glideosome-associated membrane proteins (GAPMs) also localize to the IMC but are only loosely associated with the glideosome (Bullen et al., 2009; Harding et al., 2016). Duffy binding-like MSPs (DBLMSPs), the rhoptry-associated proteins (RAPs), and the high molecular weight rhoptry proteins (RhopHs) are also important for invasion, but their precise functions are unknown (reviewed in Cowman et al., 2012) (Figure 1A).

Because invasion mechanisms are highly conserved among *Plasmodium* species (Weiss et al., 2015) and the merozoite is one of the few extracellular stages during the life cycle, proteins involved in invasion are attractive antimalarial targets. However, blocking RBC invasion is complex. The invasion process is fast

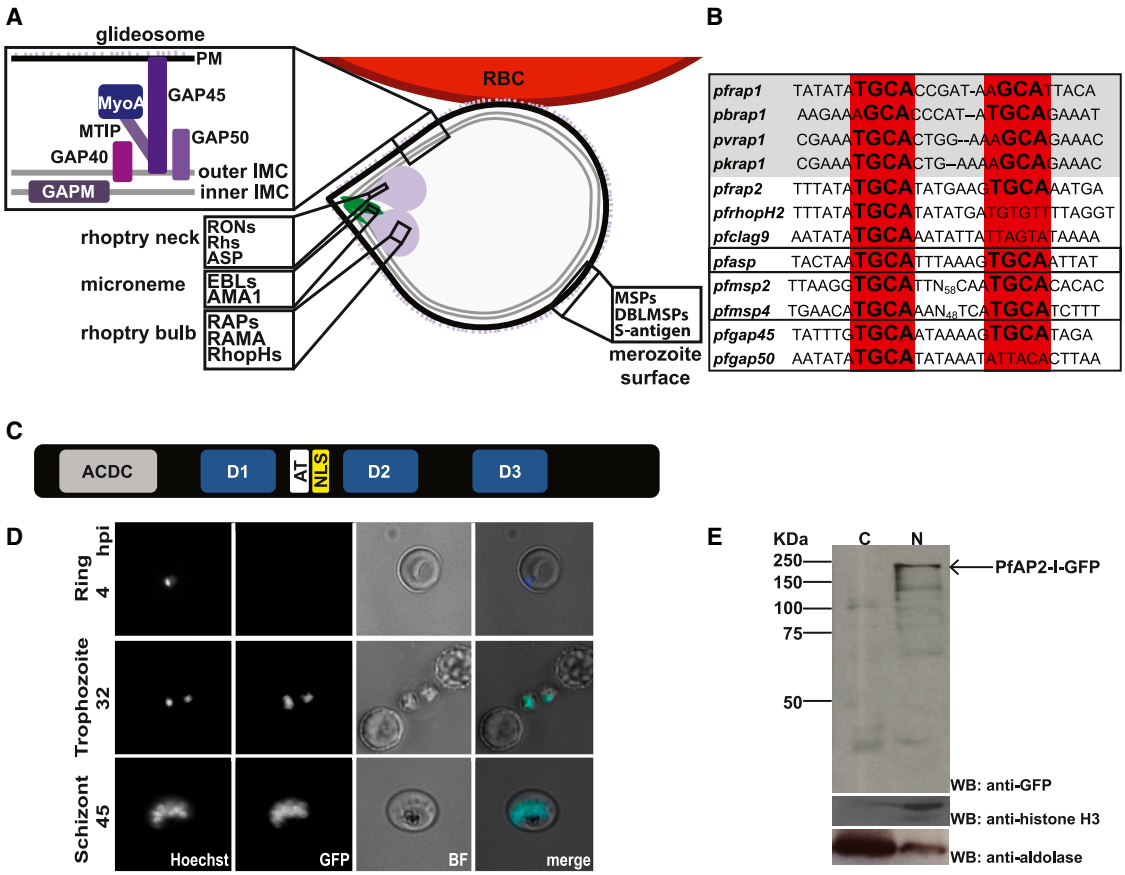

Figure 1. PfAP2-I Is a Nuclear Protein that May Bind a Conserved TGCA DNA Motif Upstream of Some Invasion Genes

(A) Merozoite attached to the RBC surface with the micronemes, rhoptries, merozoite surface, plasma membrane (PM), and inner and outer inner membrane complex (IMC) depicted. Proteins found in the glideosome, merozoite surface, microneme, rhoptry neck, and rhoptry bulb are highlighted.

(B) The NGGTGCA DNA sequence motif is conserved in invasion-related gene promoters across *P. falciparum* (Pf), *P. berghei* (Pb), *P. vivax* (Pv), or *P. knowlesi* (Pk) (gray box). The four black boxes (from top to bottom) contain rhoptry promoters, the *pfasp* rhoptry neck promoter, merozoite surface protein (*msp*) promoters, and glideosome-associated protein (*gap*) promoters (adapted from Young et al., 2008) (see also Figure S1A).

(C) The PfAP2-I protein structure contains a putative ACDC domain, the three AP2 DNA-binding domains, an AT-hook, and a nuclear localization signal (NLS) (see also Figure S2).

(D) Live fluorescence microscopy of synchronized parasites shows that PfAP2-I-GFP (see Figure S1B) localizes to the nucleus of trophozoite and schizont stage parasites but is not detected in ring stages. Hoechst was used as a nuclear marker. BF denotes bright field.

(E) Nuclear fractionation followed by western blot of schizont-stage PfAP2-I-GFP parasites confirms nuclear localization of PfAP2-I-GFP. Anti-histone H3 and anti-aldolase were used as nuclear and cytosolic markers, respectively. C, cytosol; N, nucleus.

and, with few notable exceptions, proteins that mediate parasite binding to the host RBC are functionally redundant (Walker et al., 2014). Merozoite surface proteins are also considered poor vaccine candidates because circulating merozoites express different surface variants, and the parasite can use alternative invasion pathways (reviewed in Wright and Rayner, 2014). Therefore, identifying conserved, essential invasion factors that can be therapeutically targeted remains a priority.

The expression of invasion-related genes is highly coordinated during daughter cell budding in *Plasmodium* parasites (Bozdech et al., 2003; Le Roch et al., 2003). Two conserved DNA elements are enriched upstream of invasion-related genes (Elemento et al., 2007; Essien and Stoeckert, 2010; Harris et al., 2011; Iengar and Joshi, 2009; Russell et al., 2015; Young et al., 2008). While the ACAACT motif (PfM20.1) is enriched in the promoters of micronemal genes, an NGGTGCA motif (PfM18.1) is present upstream of rhoptry genes (Young et al., 2008). The "rhoptry motif" is conserved among different *Plasmodium* species (Figures 1B and S1A) and is present upstream of the *msp* gene family and other invasion-related genes but is not found in *ron* gene promoters (with the exception of apical sushi protein, or ASP), (Figure 1B). This motif conservation implies that there are stage-specific transcription factors (TFs) that interact with these DNA motifs for expression of the invasion genes.

The ApiAP2 protein family is of plant origin and includes 27 sequence-specific DNA-binding proteins, expressed at all stages of the life cycle, each containing 1–3 AP2 DNA-binding domains (Balaji et al., 2005; Painter et al., 2011). In vitro studies have identified two AP2 domains from different ApiAP2 proteins that bind a GTGCA motif resembling the rhoptry motif (Campbell et al., 2010). The first of these proteins, PfSIP2 (PF3D7_0604100), associates uniquely with the *SPE2* motifs

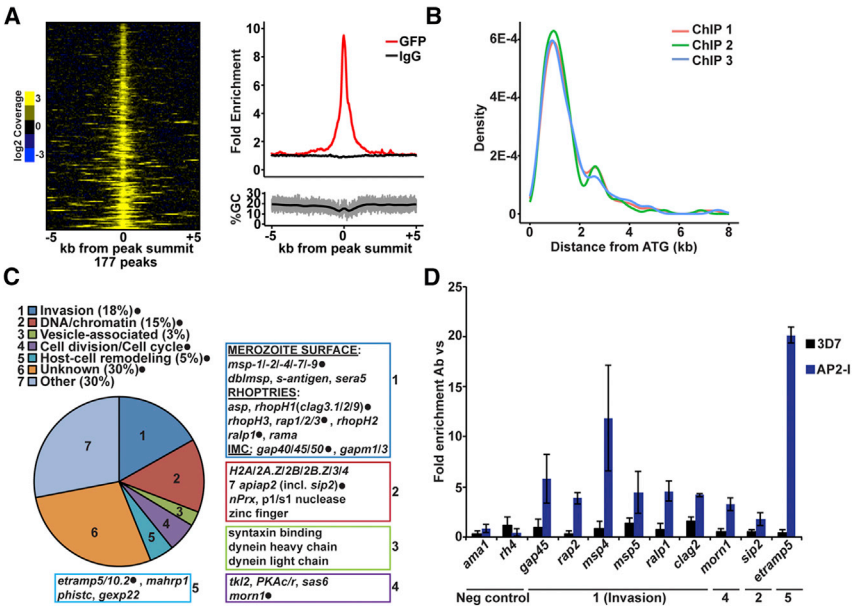

Figure 2. PfAP2-I-GFP Binds Upstream of Invasion Genes by ChIP

(A) Heatmap (left) of 165 genomic loci from ChIP-seq replicate 1, +/−5kb of each anti-GFP peak summit found in at least two of three replicates, shows enrichment of sequence reads (PfAP2-I bound) on ChIP/input samples (shown is the log2-transformed coverage). Profile plot from replicate 1 (top right) shows enrichment of anti-GFP ChIP-seq (red) compared to the control IgG ChIP-seq (black). The increase in signal is unrelated to GC content (bottom right).

(B) Plot showing the position of ChIP-seq peak summits relative to the ATG in the three replicates.

(C) Functional categorization of the 157 ChIP-seq target genes based on literature review and GO term enrichment. Annotated examples of genes belonging to each category are shown (genes tested in D are highlighted with filled black circles). For the full list of gene targets and GO term results, see Table S2.

(D) ChIP-qPCR of selected genes confirms PfAP2-I binding (blue bars) to ChIP-seq targets and no binding to the *ama1* and *rh4* promoters. Although not detected by ChIP-seq (see Figure S3D), PfAP2-I associates with *msp5* according to ChIP-qPCR. 3D7 WT parasites were used as a negative control (black bars). The results are shown as fold enrichment of ChIP performed with antibody versus non-immune IgG (n = 3). Data are represented as mean ± SD (see also Figure S3A).

found at the chromosome ends in the telomere-associated repetitive elements (TAREs) and upstream of *var* genes (Flueck et al., 2010). The second protein, PF3D7_1007700, is a 183 kDa protein, containing three AP2 domains, the third of which binds the rhoptry motif (Campbell et al., 2010). Here, we demonstrate that PF3D7_1007700 or PfAP2-I (ApiAP2 involved in invasion) is a key regulator of RBC invasion by the malaria parasite.

RESULTS

PfAP2-I Binds Upstream of Invasion-Related Genes

Homologs of the PfAP2-I protein are found across all *Plasmodium* species (Figure S2). PfAP2-I contains three conserved protein domains in addition to the three AP2 domains: an N-terminal ACDC domain (AP2-Coincident Domain mostly at the C terminus) (Iwanaga et al., 2012; Oehring et al., 2012), a putative AT-hook DNA-binding domain between the first and second AP2 domains, and a predicted nuclear localization signal (NLS) (Figures 1C and S2). Knowing that domain 3 of PfAP2-I binds the NGGTGCA rhoptry motif in vitro (Campbell et al., 2010), we sought to determine whether PfAP2-I binds this motif in vivo to regulate the transcription of invasion-related genes. First, we generated a parasite line expressing PfAP2-I C-terminally tagged with GFP (PfAP2-I-GFP) (Figure S1B). Live microscopy and nuclear fractionation assays show that PfAP2-I localizes exclusively to the nucleus of trophozoite and schizont stage parasites (Figures 1D and 1E).

To determine the genome-wide binding sites for PfAP2-I, we performed three independent chromatin immunoprecipitation assays followed by high-throughput sequencing (ChIP-seq) from PfAP2-I-GFP expressing parasites with anti-GFP or non-immune IgG antibodies. Analysis of the ChIP-seq data identified 177 regions bound by PfAP2-I in at least two of three biological replicates (Figure 2A; Table S2). These 177 regions correspond to the upstream regions of 157 genes and are largely located 1–2 kb upstream of the ATG (Figure 2B). While 30% of the PfAP2-I-bound genes encode proteins of unknown function, the largest functional group (18%) encodes known invasion proteins (Figure 2C). PfAP2-I binds to the promoters of members of the *msp*, *rap*, and *rhopH* gene families, but it does not bind upstream of micronemal or *ron* genes (Figure 2C; Table S2). Gene ontology (GO) term analysis supported the enrichment of invasion-related genes and also revealed that nucleosome and chromatin-related gene promoters are targeted by PfAP2-I (Table S2). Interestingly, PfAP2-I binds the promoters of seven *apiap2* genes (Figure 2C; Table S2), including its own, suggesting that it may auto-regulate its own gene expression. Five of these *apiap2* genes are transcribed immediately following *pfap2-I* during the IDC (Campbell et al., 2010). We also found PfAP2-I upstream of cell division/cell-cycle-related genes encoding proteins important during schizogony and genes related to vesicle formation and host cell remodeling (Figure 2C). We validated our ChIP-seq data by ChIP-qPCR and confirmed that PfAP2-I does not bind regions bound by PfSIP2 (Figures 2D and S3A) (Flueck et al., 2010). This suggests that although PfAP2-I and PfSIP2 bind a similar DNA motif in vitro (Campbell et al., 2010), they target distinct genome-wide regions. These results demonstrate that PfAP2-I is associated with the promoters of a specific set of genes that are enriched in invasion-related functions.

DNA Binding by PfAP2-I Is Important for Gene Transcription and Only Requires One AP2 Domain

Analysis of the DNA motifs enriched in the PfAP2-I ChIP-seq target gene sequences identified six DNA motifs with GTGCA

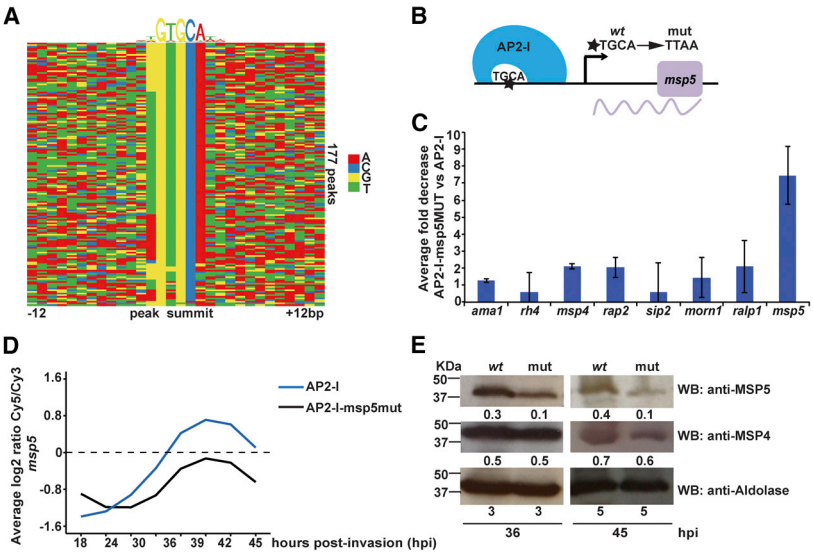

Figure 3. PfAP2-I Binding to the TGCA DNA Motif Is Important for Transcription

(A) DNA motif heatmap of the trimmed ChIP-seq peaks ± 12 bp surrounding the highest scoring motif (as discovered by DREME; Figure S3B) shows that the GTGCA DNA motif is found within the majority of the peaks. Each row represents a peak summit, and each column represents an individual nucleotide (see also Figures S3B, S3C, and S4).

(B) The mutations introduced to generate PfAP2-I-GFP::*msp5*MUT parasites (see also Figures S3D and S3E).

(C) ChIP-qPCR showing that PfAP2-I binding to *msp5* in PfAP2-I-GFP::*msp5*MUT parasites is decreased more than 7-fold versus PfAP2-I-GFP parasites. The data are represented as mean ± SD and n = 3 (see Figure S3F for original fold values).

(D) DNA microarray data using RNA extracted from PfAP2-I-GFP and PfAP2-I-GFP::*msp5*MUT parasites at eight time points beginning at 18 hpi (see Figure S3G) show that when the TGCA motif is mutated upstream of *msp5*, levels of the *msp5* transcript are reduced (see also Figures S3H and S3I). The plot shows the average of two biological replicates (see Table S3 for complete microarray results).

(E) Western blot using specific antibodies against MSP5 show that the MSP5 protein level is decreased in PfAP2-I-GFP::*msp5*MUT (mut) versus PfAP2-I-GFP (WT) parasites, but MSP4 and aldolase protein levels are unchanged at 36 and 45 hpi. Densitometry values are shown below each blot.

being the most significant (2E−25) (Figures 3A and S3B). The GTGCA motif is highly similar to the motif bound in vitro by domain 3 of PfAP2-I (Campbell et al., 2010) (Figure S3B). Four of the additional motifs are highly degenerate while a sixth, ATGCA (8E−3), is analogous to the predominant PfAP2-I motif (Figure S3B). To provide a direct link between gene transcription and binding of PfAP2-I, we tested whether mutating the GTGCA motif in a target gene promoter decreases transcription of that gene. Since *P. falciparum* is haploid and we anticipated that mutation of the motif would abolish or greatly reduce expression, this required testing a non-essential gene to maintain parasite viability. For this, we chose *pfmsp5* (*pf3d7_0206900*). This gene has previously been knocked out (Sanders et al., 2006), contains a putative PfAP2-I DNA-binding motif (ATGCA) in the promoter, and is adjacent to two PfAP2-I ChIP-seq targets (*pfmsp2* and *pfmsp4*) (Figure S3D). Although *pfmsp5* was not identified as a ChIP-seq target gene, ChIP-qPCR showed that PfAP2-I is enriched in the promoter of *pfmsp5* (Figure 2D). We used CRISPR/Cas9 to mutate the ATGCA motif in its promoter, generating the PfAP2-I-GFP::*msp5*MUT strain (Figures 3B and S3E). In this line, binding of PfAP2-I to the mutated *pfmsp5* promoter was severely reduced, as determined by ChIP-qPCR (Figures 3C and S3F). Levels of *pfmsp5* transcript were also greatly reduced, as measured by DNA microarrays and RT-qPCR (Figures 3D and S3G–S3I). Although global transcription was not affected in the mutant line, we did detect an unexpected decrease in the levels of some transcripts (Rnits p value < 5E−2) (Figure S3H; Table S3), which we hypothesize is due to compensatory regulatory mechanisms. MSP5 protein levels reflected the drop in *msp5* transcription and were decreased 3-fold (Figure 3E). PfAP2-I binding to other promoters (Figures 3C and S3F) and translation levels of the proximal invasion gene product MSP4 were not affected (Figure 3E), suggesting that PfAP2-I modulates transcription through direct and specific interaction with the TGCA DNA motif found upstream of its target genes.

The full-length PfAP2-I protein contains three AP2 DNA-binding domains that bind distinct DNA motifs in vitro (Figure 4C) (Campbell et al., 2010). Motif analysis of the 250 bp sequences surrounding each predicted ChIP-seq peak summit revealed that the DNA motifs uniquely bound by the second (D2) and third domain (D3) of PfAP2-I are prevalent in many of the ChIP-seq peaks but that the motif bound by the first AP2 domain (D1) is less common (Figures S4A and S4B). However, we failed to identify the D1 or D2 DNA motifs when performing de novo motif enrichment (Figure S3B), leading us to hypothesize that D1 and D2 were not important for in vivo DNA binding during the RBC stage. To test this, we attempted to disrupt the function of each of the three AP2 domains individually by generating parasite lines in which conserved amino acid residues were mutated to alanine using CRISPR/Cas9 mutagenesis (Figures 4A and S5A). While we were able to obtain parasites carrying mutations in AP2-I D1 (PfAP2-I-GFP-D1mut) and in AP2-I D2 (PfAP2-I-GFP-D2mut), we repeatedly failed to generate PfAP2-I-GFP-D3mut parasites (Figures S5B–S5D). Similarly, all attempts to disrupt *pfap2-i* (data not shown) or its ortholog in *P. berghei* (PBANKA_120590) (Modrzynska et al., 2017) were unsuccessful, suggesting that PfAP2-I is essential. By ChIP-qPCR, we confirmed that in the PfAP2-I-GFP-D2mut parasites, PfAP2-I was functional and remained associated to the same set of target genes as in wild-type (WT) parasites (Figure 4B). In parallel, we performed protein-binding microarrays (PBMs) (Berger and Bulyk, 2009; Campbell et al., 2010) with GST-tagged AP2-D1, AP2-D2, and AP2-D3 proteins carrying the same mutations to ensure that the introduced mutations abolished DNA binding (Figures 4C, S5C, and S5D; Table S6). Therefore, during RBC development, only the third AP2 domain of PfAP2-I, which binds GTGCA, is required to coordinate transcription.

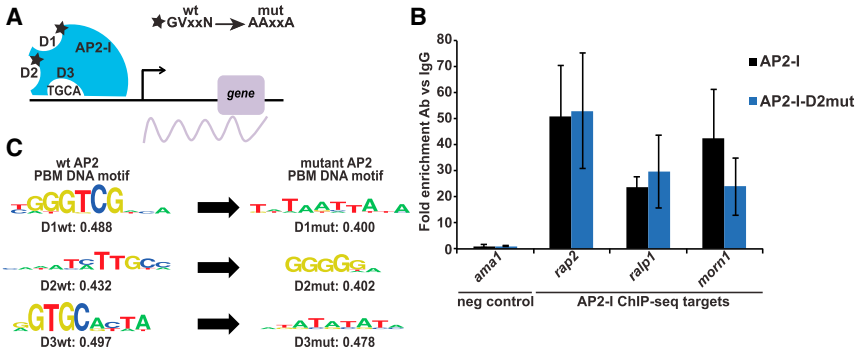

Figure 4. Only PfAP2-I-D3 Is Required for DNA Binding during the IDC

(A) The mutations introduced in the AP2 domains resulting in PfAP2-I-GFP-D1mut and PfAP2-I-GFP-D2mut parasites (see also Figures S5A–S5D).

(B) ChIP-qPCR with PfAP2-I-D2mut parasites shows that PfAP2-I still binds to its target genes when D2 is mutated (blue bars). PfAP2-I-GFP parasites were used as control (black bars). Data are represented as mean ± SD and n = 3.

(C) PBMs show that the DNA binding of PfAP2-I AP2 domains D1, D2, and D3 is altered when the domains are mutated. Shown are both WT and mutant PBM results. Enrichment values below 0.45 represent low-affinity DNA binding (see Table S6 for position weight matrices for all AP2 domains).

Gene Transcription May Require an Interaction between PfAP2-I and PfBDP1

In order to recruit the transcriptional machinery, PfAP2-I likely interacts with other proteins in the cell. To determine its interaction partners, we performed immunoaffinity purification from PfAP2-I-GFP-expressing parasites (Table S4; Figure S5G) (Joshi et al., 2013). Among the high-specificity protein interactions identified (pSAINT $\geq$ 0.9) (Figure 5A; Table S4), we found four that have been previously localized to the nucleus (Bischoff and Vaquero, 2010; Horrocks et al., 2009; Ji and Arnot, 1997; Josling et al., 2015; Templeton et al., 2004; Volz et al., 2010). These chromatin-associated proteins include bromodomain protein 1 (PfBDP1), which has been shown to positively regulate the transcription of invasion-related genes (Josling et al., 2015). Given our finding that PfBDP1 co-purified with PfAP2-I, we compared the repertoire of ChIP-seq peaks reported for PfBDP1-HA (Josling et al., 2015) to our PfAP2-I-GFP ChIP-seq results and found that 65% of PfAP2-I peaks overlap with PfBDP1-bound genomic regions (Figure 5B; Table S2). Combined with our immunoaffinity purification data, this suggests that PfAP2-I and PfBDP1 may interact in a protein complex to coordinate gene expression.

Interestingly, PfBDP1 also binds many gene promoters not bound by PfAP2-I (Figure 5B; Table S2). Our re-analysis of the published PfBDP1 ChIP-seq data (Josling et al., 2015) found that PfBDP1 is enriched at a GTGCAH motif, as reported. However, a second DNA motif (CWTAACTW), which is similar to the micronemal DNA motif (ACAACCT) (Young et al., 2008), was also identified (Figures S6B–S6D). These data suggest a model (Figure 6) in which PfAP2-I and PfBDP1 form a complex and bind the GTGCAH DNA motif to regulate the expression of rhoptry and merozoite surface genes, but not micronemal genes. ChIP-qPCR with PfBDP1-HA parasites confirmed that PfBDP1 interacts with the 5′ intergenic region of invasion genes bound by PfAP2-I but also with other invasion-related genes not associated with PfAP2-I (Figures 5C and S6A). Similarly, another protein detected by immunoaffinity purification, chromodomain protein 1 (PfCHD1), binds additional promoters besides those bound by PfAP2-I, as determined by ChIP-qPCR using PfCHD1-GFP parasites (Volz et al., 2010) (Figures 5C and S6A). Therefore, although PfBDP1 and PfCHD1 likely associate with PfAP2-I, they may also be independently recruited to chromatin through other DNA-binding proteins.

To determine the temporal association of the PfAP2-I/PfBDP1 complex on the chromatin, we explored whether PfAP2-I binds to the invasion promoters before or after PfBDP1. First, we tested whether PfAP2-I and/or PfBDP1 were bound to the promoters at the trophozoite stage prior to transcription of the target genes. Indeed PfAP2-I binds to the target gene promoters at the trophozoite stage (22 hr post-invasion) and remains associated in schizonts (40 hr post-invasion). However, PfBDP1, as previously shown (Josling et al., 2015), does not bind at the trophozoite stage and only binds at the later time point (Figures 7A and S7A). We then pursued a knockdown strategy to test DNA binding in the absence of one of the two proteins. While we were unable to generate a PfAP2-I knockdown (data not shown), PfBDP1 has been previously knocked down using the FK506-binding protein (FKBP) destabilization domain (DD) system (PfBDP1-HA-DD) (Josling et al., 2015). In these parasites, PfBDP1 is fused to DD, which is stabilized only in the presence of the small molecule ligand Shld-1 (Armstrong and Goldberg, 2007). PfBDP1-HA-DD parasites grown in the absence of Shld-1 invade RBCs poorly due to the reduced expression of invasion genes (Josling et al., 2015). To study the interaction between PfAP2-I and PfBDP1, we recreated the PfBDP1 knockdown in the PfAP2-I-GFP background (PfAP2-I-GFP::PfBDP1-HA-DD) (Figures 7B and S7B). ChIP-qPCR assays with these parasites demonstrate that PfAP2-I is bound to the target genes (Figures 7C and 7D) in the absence of PfBDP1 (minus Shld-1), supporting a model in which PfAP2-I binds the promoters of specific invasion genes before PfBDP1 recruitment to the same regions (Figure 6).

DISCUSSION

In *Plasmodium* parasites, gene transcription is highly periodic, with maximal transcript levels reached only once during the 48 hr IDC. Late in the IDC, the parasite induces the transcription of genes encoding proteins involved in RBC invasion (Bozdech et al., 2003; Le Roch et al., 2004). Two DNA elements are enriched in the promoters of invasion genes; ACAACT is present in the promoters of genes encoding micronemal and RON proteins and NGGTGCA is associated with the promoters of rhoptry bulb, *msp*, and some glideosome genes (Elemento et al., 2007; Essien and Stoeckert, 2010; Harris et al., 2011; Iengar and Joshi, 2009; Russell et al., 2015; Young et al., 2008). Based on in vitro DNA-binding data (Campbell et al., 2010), we hypothesized that PfAP2-I binds the NGGTGCA DNA motif and drives expression of invasion-related genes.

A

PlasmoDB ID	Protein description	pSAINT
PF3D7_1023900	Chromodomain-helicase-DNA-binding protein 1 homolog (CHD1)	1
PF3D7_0624600	Smarca-related protein (ISWI)	1
PF3D7_1133200	Conserved Plasmodium protein	1
PF3D7_0517400	Transcriptional regulator, putative (FACT-L)	0.99
PF3D7_1033700	Bromodomain protein 1 (BDP1)	0.99
PF3D7_1130700	Structural maintenance of chromosome protein, putative (SMC)	0.95
PF3D7_1441400	Structure specific recognition protein (FACT-S)	0.95

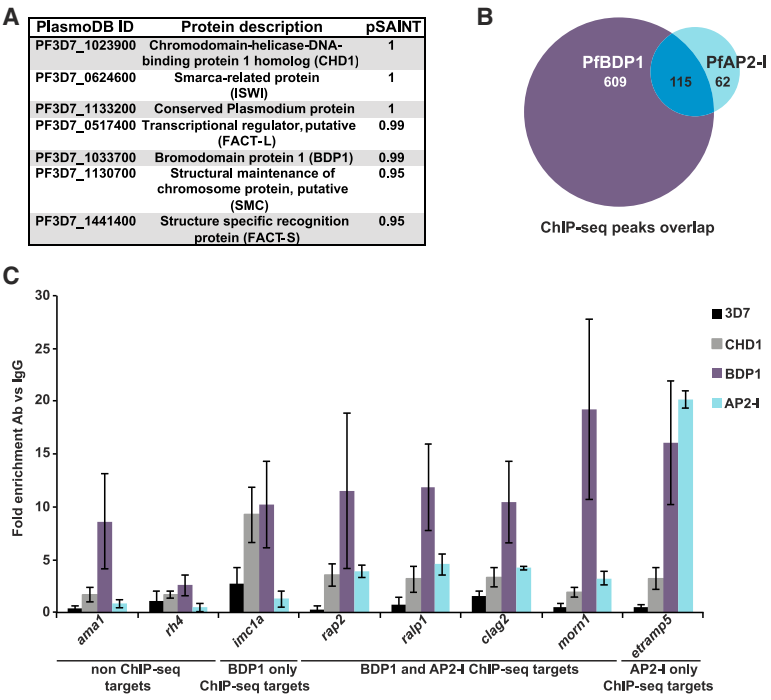

Figure 5. PfAP2-I and PfBDP1 Co-immunoprecipitate and Regulate Transcription of Many of the Same Genes

(A) List of PfAP2-I interaction partners with probability of interaction as measured by SAINT (pSAINT) of 0.9 or above (see also Figure S6A; for full list of proteins detected, see Table S4).

(B) Venn diagram comparing the peaks found by ChIP-seq for PfBDP1-HA (Josling et al., 2015) (purple) and PfAP2-I-GFP (this study) (light blue) shows that 115 genomic regions are bound by both proteins. See also Table S2.

(C) ChIP-qPCR of PfAP2-I-GFP, PfBDP1-HA, and PfCHD1-GFP confirms that PfAP2-I does not bind genes only found in the PfBDP1 ChIP-seq dataset. Data are represented as mean ± SD and n = 4 (see also Figure S6B, which shows some of the same data).

By ChIP-seq, we have shown that PfAP2-I is enriched at the promoters of invasion genes, binding to 45 genes from a previously generated "invasion list" (Bozdech et al., 2003) and 63 genes from a predicted "invadome" subnetwork (Hu et al., 2010) (Table S5). Furthermore, many of the genes bound by PfAP2-I are expressed at the mid- to late-schizont stage since 40% of the target genes are included in either a schizont-specific or an invasion-related microarray expression cluster (Le Roch et al., 2003) (Table S5). We predict that many of the PfAP2-I target genes encoding proteins of unknown function (30% of total) may also have unrecognized functions during invasion and merozoite development.

Notably, genes encoding known invasion protein complexes are co-regulated by PfAP2-I. For example, PfRAP2 interacts with PfRAP3, which is escorted to the rhoptries via interaction with PfRAP1 (Baldi et al., 2000) and is itself escorted via association with the rhoptry-associated membrane antigen (PfRAMA) protein (Richard et al., 2009). PfAP2-I binds the promoters of all four of these genes. Similarly, PfAP2-I binds upstream of *pfmsp1* and *pfmps7*, and PfMSP1 is known to interact with PfMSP6 and PfMSP7 (Pachebat et al., 2001; Trucco et al., 2001). Genes encoding glideosome proteins PfGAP40/45/50 are also PfAP2-I targets. The absence of the GTGCA motif and lack of PfAP2-I binding to micronemal and *ron* gene promoters indicates that genes encoding for proteins involved in invasion stages post-RBC recognition, such as PfAMA1, RONs, EBLs, or Rhs, are likely transcribed by an unidentified TF that may bind the micronemal ACAACT motif present upstream of these genes (Young et al., 2008). PfAP2-I also binds upstream of genes encoding the cAMP-dependent protein kinase regulatory and catalytic subunits (PKA-r and -c), which regulate microneme secretion prior to invasion (Dawn et al., 2014). Interestingly, cytoadherence-linked asexual gene (CLAG) proteins are also targets of PfAP2-I. Although the CLAGs are members of the RhopH protein family, they are not involved in invasion, but their expression matches that of invasion-related genes (Counihan et al., 2017; Ito et al., 2017; Sherling et al., 2017).

Previous in vitro DNA-binding experiments have predicted that PfAP2-I regulates the expression of nucleosome-related genes (Campbell et al., 2010). Our ChIP-seq data confirmed that PfAP2-I binds the promoter regions of most histone genes, as well as seven *apiap2* genes, including *pfap2-I* and five *apiap2* genes that are transcribed later than *pfap2-I*. Among the *apiap2* target genes, only PfSIP2 (Flueck et al., 2010) and PfAP2-G (Kafsack et al., 2014; Sinha et al., 2014) have been functionally characterized. A third ApiAP2 protein, PF3D7_1107800, may be part of an actin protein complex participating in nuclear repositioning of *var* genes (Zhang et al., 2011). The identification of other *apiap2* genes as PfAP2-I targets provides evidence for ApiAP2 proteins functioning in a transcriptional regulatory network. PfAP2-I also associates with the promoters of known cell division-related genes. These include dynein light and heavy chain (PfDLC and PfDHC) (reviewed in Striepen et al., 2007), cartwheel protein PfSas-6 (Suvorova et al., 2015), and MORN-repeat containing

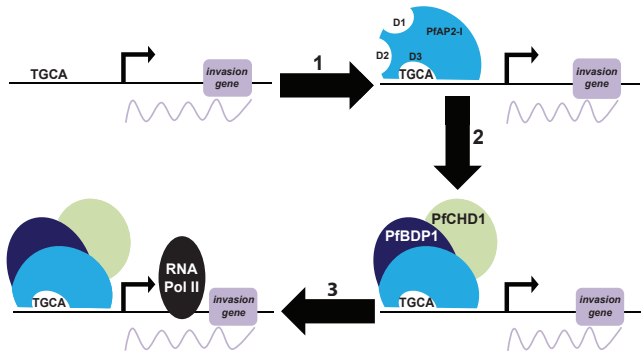

Figure 6. Model of transcription regulation by PfAP2-I and PfBDP1

Our model is that PfAP2-I must first bind the TGCA DNA motif within the promoters of invasion genes via its third AP2 domain (D3). Subsequently, PfBDP1 and PfCHD1 are recruited followed by RNA polymerase II, thereby initiating transcription.

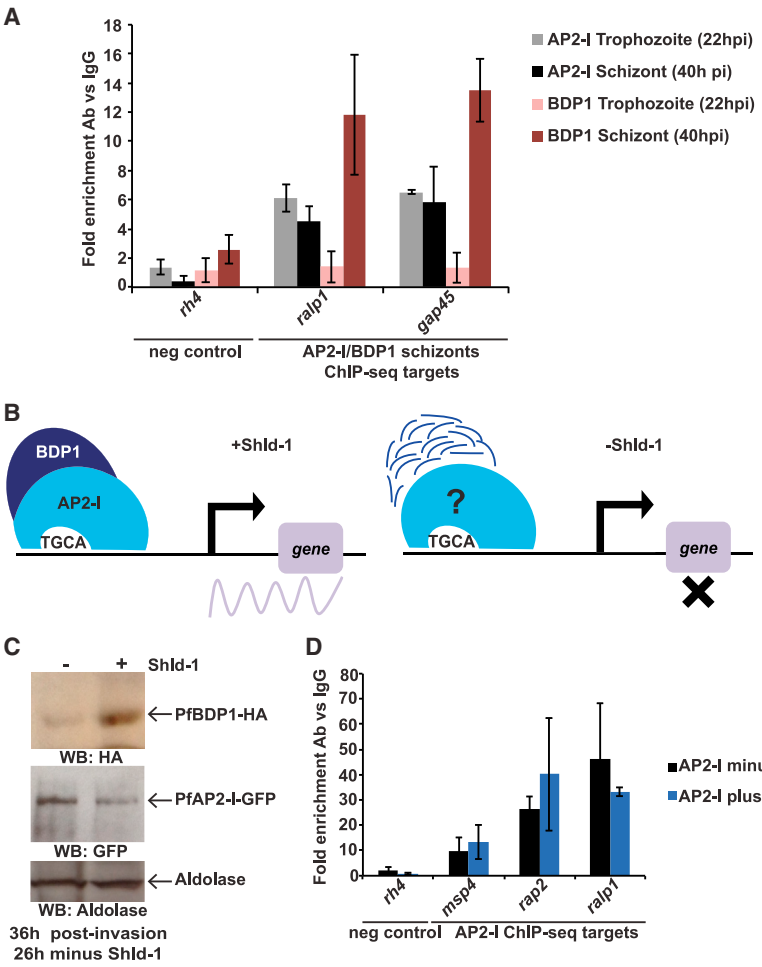

Figure 7. PfAP2-I Binding Precedes PfBDP1 Binding to the Target Gene Promoters

(A) ChIP-qPCR demonstrates that PfAP2-I-GFP, but not PfBDP1-HA, is already bound to its target promoters at 22 hpi. Data are represented as mean ± SD and n = 2. The schizont data are the same as in Figure S6B. (For PfBDP1 ChIP positive control, see Figure S7A.)

(B) In the presence of Shld-1, there are wild-type levels of PfBDP1, but in the absence of Shld-1, PfBDP1-DD is degraded and target gene transcription cannot be initiated (Josling et al., 2015). PfAP2-I may or may not remain associated to the TGCA DNA motif in the absence of PfBDP1.

(C) Western blot of schizont-stage PfAP2-I-GFP::PfBDP1-HA-DD parasites shows that, while the protein levels of PfAP2-I-GFP remain identical in the presence or absence of Shld-1, PfBDP1-DD protein levels are reduced in the absence of Shld-1. Anti-aldolase was used as a loading control.

(D) ChIP-qPCR shows that in PfAP2-I-GFP::PfBDP1-HA-DD parasites (see Figure S7), PfAP2-I-GFP remains bound to the target gene promoters even when PfBDP1 is knocked down (−Shld-1). Data are represented as mean ± SD and n = 3. *rh4* was used as negative control for DNA binding.

protein 1 (PfMORN1) (Heaslip et al., 2010; Lorestani et al., 2010). Genes encoding proteins involved in RBC remodeling are also targets of PfAP2-I, namely early transcribed membrane proteins (ETRAMPs) 5 and 10.2 (Spielmann et al., 2003) and membrane-associated histidine rich protein 1 (PfMAHRP1) (Spycher et al., 2008).

The GTGCA DNA motif is highly enriched in our ChIP-seq data. PfAP2-I binding to GTGCA is important for transcription since mutation of this DNA motif upstream of *msp5* affects PfAP2-I binding and gene expression (Figures 3B–3E), strongly indicating that PfAP2-I is the TF responsible for transcribing *msp5*. While binding of PfAP2-I D3 to the GTGCA DNA sequence is essential, parasites carrying mutations that abrogate DNA binding of D1 or D2 are viable, indicating that D3 is sufficient to mediate DNA binding during the RBC stage (Figure 4). We hypothesize that D3 may be a stronger DNA binder or that protein domains in proximity to the other AP2 domains influence DNA binding. Indeed, PBM binding of the PfAP2-I AT-hook domain fused to D2 (AT-D2) did not recapitulate binding of D2 alone but rather that of the AT-hook (AT) (Figures S5E and S5F; Table S6). Post-translational modification of the AP2 domains might also alter DNA binding; D2 is acetylated during the late stages of the IDC when PfAP2-I binds the target genes and an acetylation mimic of D2 cannot bind DNA by PBM (Cobbold et al., 2016).

Another possibility is that D1 and D2 are important at other stages of the life cycle; PfAP2-I is also expressed in ookinetes (López-Barragán et al., 2011) and its *P. yoelii* ortholog (PY17X_1209100) is expressed in sporozoites (Lindner et al., 2013).

Our immunoaffinity purification experiments found that PfAP2-I co-purifies with proteins previously identified in a nuclear proteome (Oehring et al., 2012). ChIP-qPCR suggests that PfAP2-I binds to its target genes in a complex with PfCHD1 and PfBDP1. PfBDP1 has previously been shown to regulate transcription of invasion-related genes and to be required for host cell invasion. However, although PfBDP1 binds H3K9ac in vitro, this alone cannot explain how PfBDP1 is recruited to target genes as H3K9ac is much more widely distributed in the genome than is PfBDP1 (Josling et al., 2015). Our data indicate that PfAP2-I DNA binding precedes recruitment of PfBDP1, and we speculate that PfBDP1 transcriptional activity may require interaction with TFs (such as PfAP2-I) that can directly recognize specific DNA motifs across the genome. In accordance with this model, we suggest that PfAP2-I first binds to NGGTGCA DNA motifs and recruits PfBDP1 (Figure 6) and that interaction with an unidentified TF also enables PfBDP1 recruitment to the CWTAACTW DNA motif. Our results show that when PfBDP1 protein levels are knocked down, PfAP2-I remains associated to its target gene promoters and, as shown in Josling et al. (2015), their transcript levels are reduced. We propose that PfAP2-I DNA binding is not sufficient to induce gene transcription and requires interaction with PfBDP1. This is similar to what is seen in human cells, where some TFs can only transcribe target genes when interacting with bromodomain proteins (reviewed in Shi and Vakoc, 2014). Such interactions occur through the association of the

bromodomain with acetylated lysines in the TFs or via association of the phosphorylated bromodomain to the TFs. Intriguingly, PfAP2-I is acetylated at the trophozoite stage (Cobbold et al., 2016) and PfBDP1 is phosphorylated (reviewed in Doerig et al., 2015). In addition to a bromodomain, PfBDP1 also has three ankyrin repeats (Aravind et al., 2003), which may be involved in protein-protein interactions. Thus, further experimentation is required to determine how PfAP2-I binding to GTGCA DNA motifs and interaction with PfBDP1mediates transcription of invasion genes (Figure 6). Overall, our data suggest that PfAP2-I plays a key role in the transcription of a subset of invasion genes by recruiting the bromodomain protein PfBDP1 and thus that PfAP2-I may be a potential therapeutic target.

STAR★METHODS

Detailed methods are provided in the online version of this paper and include the following:

- KEY RESOURCES TABLE
- CONTACT FOR REAGENT AND RESOURCE SHARING
- EXPERIMENTAL MODEL AND SUBJECT DETAILS
  - Parasite Culture and Transfection
  - Parasite Strains
  - Bacterial Strains
- METHOD DETAILS
  - *P. falciparum* Transfections
  - Antibodies
  - Plasmid DNA Cloning
  - Expression and Purification of Recombinant Proteins
  - Protein Binding Microarrays
  - Bioinformatic Searches
  - Nuclear Fractionation Assays and Western Blot
  - Immunoaffinity Purification Assays
  - DNA Microarrays
  - ChIP-Seq
  - ChIP-qPCR
  - RT-qPCR
- QUANTIFICATION AND STATISTICAL ANALYSIS
  - Western Blot Protein Quantification
  - ChIP-qPCR and RT-PCR Data Analysis
  - DNA Microarrays
  - Protein Binding Microarrays
  - ChIP-Seq Data Analysis
  - Immunoaffinity Purification
- DATA AND SOFTWARE AVAILABILITY
  - ChIP-Seq Data
  - DNA Microarray Data
  - Protein Data
  - Protein Binding Microarray Data

SUPPLEMENTAL INFORMATION

Supplemental Information includes seven figures and six tables and can be found with this article online at http://dx.doi.org/10.1016/j.chom.2017.05.006.

AUTHOR CONTRIBUTIONS

J.M.S. and M.L. conceived the experiments and wrote the manuscript. T.C. generated the PfAP2-I-GFP parasite line and initiated the project. I.M.C. contributed protocols and reagents to the immunoaffinity purification proteomic studies, and P.J. performed and analyzed some of the immunoaffinity purification experiments. A.S. performed PBMs, L.O. ran DNA microarrays and PBMs, G.J. performed RT-qPCR and ChIP assays, and P.R. handled all bioinformatic data analysis. J.M.S. performed all other experiments. All authors have read the manuscript.

ACKNOWLEDGMENTS

J.M.S. is a recipient of Swiss National Fund GEP3-13613 and EMBO Long-Term Fellowship 633-2011, T.L.C. was funded by an NSERC Postdoctoral Fellowship, J.P. was funded by an NJCCR postdoctoral fellowship, and G.J. is the recipient of an American Heart Association Postdoctoral Research Grant 16POST26420067. This work was funded by NIH/NIAID R01AI076276 (M.L.) and R01AI125565 (M.L.), the Arnold and Mabel Beckman Foundation (002375), and support from the Center for Quantitative Biology (P50 GM071508) (M.L.) and R01GM114141 (I.M.C.). We thank the Voss (SIP2N-HA), Cowman (CHD1-GFP), and Duffy (BDP1-HA) labs for sharing parasite strains. We thank Dr. T. Greco in the Cristea lab for the mass spectrometric analysis at Princeton University and Dr. T. Laremore for those performed at the Pennsylvania State University in the Huck Proteomics and Mass Spectrometry Core Facility. We thank Dr. T. Otto, Dr. M. Berriman, and Dr. U. Boehme from the UK Wellcome Trust Sanger Institute for use of the Pf Dd2 draft annotations from the Pf3K project. We thank Dr. H. Painter for help with Rnits, discussions of the data, and critical reading of the manuscript. We thank A. Minns for assistance with protein quantification. High-throughput sequencing analyses were performed at the Huck Genomics Core Facility, University Park, PA. The anti-MSP4 and anti-MSP5 antibodies were obtained through the MR4 as part of the BEI resources repository.

Received: March 7, 2016
Revised: February 16, 2017
Accepted: May 23, 2017
Published: June 14, 2017

REFERENCES

Andrew, S. (2010). FASTQC: a quality control tool for high throughput sequence data (Babraham Institute), http://www.bioinformatics.babraham.ac.uk/projects/fastqc/.

Aravind, L., Iyer, L.M., Wellems, T.E., and Miller, L.H. (2003). *Plasmodium* biology: genomic gleanings. Cell *115*, 771–785.

Armstrong, C.M., and Goldberg, D.E. (2007). An FKBP destabilization domain modulates protein levels in *Plasmodium falciparum*. Nat. Methods *4*, 1007–1009.

Aurrecoechea, C., Brestelli, J., Brunk, B.P., Dommer, J., Fischer, S., Gajria, B., Gao, X., Gingle, A., Grant, G., Harb, O.S., et al. (2009). PlasmoDB: a functional genomic database for malaria parasites. Nucleic Acids Res. *37*, D539–D543.

Bailey, T.L. (2011). DREME: motif discovery in transcription factor ChIP-seq data. Bioinformatics *27*, 1653–1659.

Balaji, S., Babu, M.M., Iyer, L.M., and Aravind, L. (2005). Discovery of the principal specific transcription factors of Apicomplexa and their implication for the evolution of the AP2-integrase DNA binding domains. Nucleic Acids Res. *33*, 3994–4006.

Baldi, D.L., Andrews, K.T., Waller, R.F., Roos, D.S., Howard, R.F., Crabb, B.S., and Cowman, A.F. (2000). RAP1 controls rhoptry targeting of RAP2 in the malaria parasite *Plasmodium falciparum*. EMBO J. *19*, 2435–2443.

Bembom, O. (2017). seqLogo: Sequence logos for DNA sequence alignments. R package version 1.42.0. (Bioconductor).

Berger, M.F., and Bulyk, M.L. (2009). Universal protein-binding microarrays for the comprehensive characterization of the DNA-binding specificities of transcription factors. Nat. Protoc. *4*, 393–411.

Bischoff, E., and Vaquero, C. (2010). *In silico* and biological survey of transcription-associated proteins implicated in the transcriptional machinery during the erythrocytic development of *Plasmodium falciparum*. BMC Genomics *11*, 34.

Bolger, A.M., Lohse, M., and Usadel, B. (2014). Trimmomatic: a flexible trimmer for Illumina sequence data. Bioinformatics *30*, 2114–2120.

Bozdech, Z., Llinás, M., Pulliam, B.L., Wong, E.D., Zhu, J., and DeRisi, J.L. (2003). The transcriptome of the intraerythrocytic developmental cycle of *Plasmodium falciparum*. PLoS Biol. *1*, E5.

Braun-Breton, C., Rosenberry, T.L., and da Silva, L.P. (1988). Induction of the proteolytic activity of a membrane protein in *Plasmodium falciparum* by phosphatidyl inositol-specific phospholipase C. Nature *332*, 457–459.

Bullen, H.E., Tonkin, C.J., O'Donnell, R.A., Tham, W.H., Papenfuss, A.T., Gould, S., Cowman, A.F., Crabb, B.S., and Gilson, P.R. (2009). A novel family of Apicomplexan glideosome-associated proteins with an inner membrane-anchoring role. J. Biol. Chem. *284*, 25353–25363.

Campbell, T.L., De Silva, E.K., Olszewski, K.L., Elemento, O., and Llinás, M. (2010). Identification and genome-wide prediction of DNA binding specificities for the ApiAP2 family of regulators from the malaria parasite. PLoS Pathog. *6*, e1001165.

Choi, H., Larsen, B., Lin, Z.Y., Breitkreutz, A., Mellacheruvu, D., Fermin, D., Qin, Z.S., Tyers, M., Gingras, A.C., and Nesvizhskii, A.I. (2011). SAINT: probabilistic scoring of affinity purification-mass spectrometry data. Nat. Methods *8*, 70–73.

Cobbold, S.A., Santos, J.M., Ochoa, A., Perlman, D.H., and Llinás, M. (2016). Proteome-wide analysis reveals widespread lysine acetylation of major protein complexes in the malaria parasite. Sci. Rep. *6*, 19722.

Combe, A., Giovannini, D., Carvalho, T.G., Spath, S., Boisson, B., Loussert, C., Thiberge, S., Lacroix, C., Gueirard, P., and Ménard, R. (2009). Clonal conditional mutagenesis in malaria parasites. Cell Host Microbe *5*, 386–396.

Corpet, F. (1988). Multiple sequence alignment with hierarchical clustering. Nucleic Acids Res. *16*, 10881–10890.

Counihan, N.A., Chisholm, S.A., Bullen, H.E., Srivastava, A., Sanders, P.R., Jonsdottir, T.K., Weiss, G.E., Ghosh, S., Crabb, B.S., Creek, D.J., et al. (2017). *Plasmodium falciparum* parasites deploy RhopH2 into the host erythrocyte to obtain nutrients, grow and replicate. Elife *6*, 6.

Cowman, A.F., Berry, D., and Baum, J. (2012). The cellular and molecular basis for malaria parasite invasion of the human red blood cell. J. Cell Biol. *198*, 961–971.

Cristea, I.M., Williams, R., Chait, B.T., and Rout, M.P. (2005). Fluorescent proteins as proteomic probes. Mol. Cell. Proteomics *4*, 1933–1941.

Crowley, V.M., Rovira-Graells, N., Ribas de Pouplana, L., and Cortés, A. (2011). Heterochromatin formation in bistable chromatin domains controls the epigenetic repression of clonally variant Plasmodium falciparum genes linked to erythrocyte invasion. Mol. Microbiol. *80*, 391–406.

Dale, R.K., Pedersen, B.S., and Quinlan, A.R. (2011). Pybedtools: a flexible Python library for manipulating genomic datasets and annotations. Bioinformatics *27*, 3423–3424.

Das, S., Hertrich, N., Perrin, A.J., Withers-Martinez, C., Collins, C.R., Jones, M.L., Watermeyer, J.M., Fobes, E.T., Martin, S.R., Saibil, H.R., et al. (2015). Processing of *Plasmodium falciparum* merozoite surface protein MSP1 activates a spectrin-binding function enabling parasite egress from RBCs. Cell Host Microbe *18*, 433–444.

Dawn, A., Singh, S., More, K.R., Siddiqui, F.A., Pachikara, N., Ramdani, G., Langsley, G., and Chitnis, C.E. (2014). The central role of cAMP in regulating *Plasmodium falciparum* merozoite invasion of human erythrocytes. PLoS Pathog. *10*, e1004520.

Doerig, C., Rayner, J.C., Scherf, A., and Tobin, A.B. (2015). Post-translational protein modifications in malaria parasites. Nat. Rev. Microbiol. *13*, 160–172.

Dvorin, J.D., Martyn, D.C., Patel, S.D., Grimley, J.S., Collins, C.R., Hopp, C.S., Bright, A.T., Westenberger, S., Winzeler, E., Blackman, M.J., et al. (2010). A plant-like kinase in *Plasmodium falciparum* regulates parasite egress from erythrocytes. Science *328*, 910–912.

Elemento, O., Slonim, N., and Tavazoie, S. (2007). A universal framework for regulatory element discovery across all genomes and data types. Mol. Cell *28*, 337–350.

Eng, J.K., McCormack, A.L., and Yates, J.R. (1994). An approach to correlate tandem mass spectral data of peptides with amino acid sequences in a protein database. J. Am. Soc. Mass Spectrom. *5*, 976–989.

Essien, K., and Stoeckert, C.J., Jr. (2010). Conservation and divergence of known apicomplexan transcriptional regulons. BMC Genomics *11*, 147.

Fidock, D.A., and Wellems, T.E. (1997). Transformation with human dihydrofolate reductase renders malaria parasites insensitive to WR99210 but does not affect the intrinsic activity of proguanil. Proc. Natl. Acad. Sci. USA *94*, 10931–10936.

Fidock, D.A., Nomura, T., Talley, A.K., Cooper, R.A., Dzekunov, S.M., Ferdig, M.T., Ursos, L.M., Sidhu, A.B., Naudé, B., Deitsch, K.W., et al. (2000). Mutations in the *P. falciparum* digestive vacuole transmembrane protein PfCRT and evidence for their role in chloroquine resistance. Mol. Cell *6*, 861–871.

Flueck, C., Bartfai, R., Volz, J., Niederwieser, I., Salcedo-Amaya, A.M., Alako, B.T., Ehlgen, F., Ralph, S.A., Cowman, A.F., Bozdech, Z., et al. (2009). *Plasmodium falciparum* heterochromatin protein 1 marks genomic loci linked to phenotypic variation of exported virulence factors. PLoS Pathog. *5*, e1000569.

Flueck, C., Bartfai, R., Niederwieser, I., Witmer, K., Alako, B.T., Moes, S., Bozdech, Z., Jenoe, P., Stunnenberg, H.G., and Voss, T.S. (2010). A major role for the *Plasmodium falciparum* ApiAP2 protein PfSIP2 in chromosome end biology. PLoS Pathog. *6*, e1000784.

Frénal, K., Polonais, V., Marq, J.B., Stratmann, R., Limenitakis, J., and Soldati-Favre, D. (2010). Functional dissection of the apicomplexan glideosome molecular architecture. Cell Host Microbe *8*, 343–357.

Gao, X., Gunalan, K., Yap, S.S., and Preiser, P.R. (2013). Triggers of key calcium signals during erythrocyte invasion by *Plasmodium falciparum*. Nat. Commun. *4*, 2862.

Ghorbal, M., Gorman, M., Macpherson, C.R., Martins, R.M., Scherf, A., and Lopez-Rubio, J.J. (2014). Genome editing in the human malaria parasite *Plasmodium falciparum* using the CRISPR-Cas9 system. Nat. Biotechnol. *32*, 819–821.

Grant, C.E., Bailey, T.L., and Noble, W.S. (2011). FIMO: scanning for occurrences of a given motif. Bioinformatics *27*, 1017–1018.

Greco, T.M., Miteva, Y., Conlon, F.L., and Cristea, I.M. (2012). Complementary proteomic analysis of protein complexes. Methods Mol. Biol. *917*, 391–407.

Gupta, S., Stamatoyannopoulos, J.A., Bailey, T.L., and Noble, W.S. (2007). Quantifying similarity between motifs. Genome Biol. *8*, R24.

Han, C.L., Chien, C.W., Chen, W.C., Chen, Y.R., Wu, C.P., Li, H., and Chen, Y.J. (2008). A multiplexed quantitative strategy for membrane proteomics: opportunities for mining therapeutic targets for autosomal dominant polycystic kidney disease. Mol. Cell. Proteomics *7*, 1983–1997.

Harding, C.R., Egarter, S., Gow, M., Jiménez-Ruiz, E., Ferguson, D.J., and Meissner, M. (2016). Gliding associated proteins play essential roles during the formation of the inner membrane complex of *Toxoplasma gondii*. PLoS Pathog. *12*, e1005403.

Harris, E.Y., Ponts, N., Le Roch, K.G., and Lonardi, S. (2011). Chromatin-driven *de novo* discovery of DNA binding motifs in the human malaria parasite. BMC Genomics *12*, 601.

Heaslip, A.T., Dzierszinski, F., Stein, B., and Hu, K. (2010). TgMORN1 is a key organizer for the basal complex of *Toxoplasma gondii*. PLoS Pathog. *6*, e1000754.

Horrocks, P., Wong, E., Russell, K., and Emes, R.D. (2009). Control of gene expression in *Plasmodium falciparum* - ten years on. Mol. Biochem. Parasitol. *164*, 9–25.

Hu, G., Cabrera, A., Kono, M., Mok, S., Chaal, B.K., Haase, S., Engelberg, K., Cheemadan, S., Spielmann, T., Preiser, P.R., et al. (2010). Transcriptional profiling of growth perturbations of the human malaria parasite *Plasmodium falciparum*. Nat. Biotechnol. *28*, 91–98.

Hume, M.A., Barrera, L.A., Gisselbrecht, S.S., and Bulyk, M.L. (2015). UniPROBE, update 2015: new tools and content for the online database of protein-binding microarray data on protein-DNA interactions. Nucleic Acids Res. *43*, D117–D122.

Iengar, P., and Joshi, N.V. (2009). Identification of putative regulatory motifs in the upstream regions of co-expressed functional groups of genes in *Plasmodium falciparum*. BMC Genomics *10*, 18.

Ito, D., Schureck, M.A., and Desai, S.A. (2017). An essential dual-function complex mediates erythrocyte invasion and channel-mediated nutrient uptake in malaria parasites. Elife *6*, 6.

Iwanaga, S., Kaneko, I., Kato, T., and Yuda, M. (2012). Identification of an AP2-family protein that is critical for malaria liver stage development. PLoS One *7*, e47557.

Ji, D.D., and Arnot, D.E. (1997). A *Plasmodium falciparum* homologue of the ATPase subunit of a multi-protein complex involved in chromatin remodelling for transcription. Mol. Biochem. Parasitol. *88*, 151–162.

Joshi, P., Greco, T.M., Guise, A.J., Luo, Y., Yu, F., Nesvizhskii, A.I., and Cristea, I.M. (2013). The functional interactome landscape of the human histone deacetylase family. Mol. Syst. Biol. *9*, 672.

Josling, G.A., Petter, M., Oehring, S.C., Gupta, A.P., Dietz, O., Wilson, D.W., Schubert, T., Längst, G., Gilson, P.R., Crabb, B.S., et al. (2015). A *Plasmodium Falciparum* bromodomain protein regulates invasion gene expression. Cell Host Microbe *17*, 741–751.

Kadekoppala, M., Kline, K., Akompong, T., and Haldar, K. (2000). Stable expression of a new chimeric fluorescent reporter in the human malaria parasite *Plasmodium falciparum*. Infect. Immun. *68*, 2328–2332.

Kafsack, B.F., Rovira-Graells, N., Clark, T.G., Bancells, C., Crowley, V.M., Campino, S.G., Williams, A.E., Drought, L.G., Kwiatkowski, D.P., Baker, D.A., et al. (2014). A transcriptional switch underlies commitment to sexual development in malaria parasites. Nature *507*, 248–252.

Le Roch, K.G., Zhou, Y., Blair, P.L., Grainger, M., Moch, J.K., Haynes, J.D., De La Vega, P., Holder, A.A., Batalov, S., Carucci, D.J., and Winzeler, E.A. (2003). Discovery of gene function by expression profiling of the malaria parasite life cycle. Science *301*, 1503–1508.

Le Roch, K.G., Johnson, J.R., Florens, L., Zhou, Y., Santrosyan, A., Grainger, M., Yan, S.F., Williamson, K.C., Holder, A.A., Carucci, D.J., et al. (2004). Global analysis of transcript and protein levels across the *Plasmodium falciparum* life cycle. Genome Res. *14*, 2308–2318.

Letunic, I., Doerks, T., and Bork, P. (2012). SMART 7: recent updates to the protein domain annotation resource. Nucleic Acids Res. *40*, D302–D305.

Li, H. (2013). Aligning sequence reads, clone sequences and assembly contigs with BWA-MEM. arXiv, arXiv:13033997v2, https://arxiv.org/abs/1303.3997.

Li, H., Handsaker, B., Wysoker, A., Fennell, T., Ruan, J., Homer, N., Marth, G., Abecasis, G., and Durbin, R.; 1000 Genome Project Data Processing Subgroup (2009). The Sequence Alignment/Map format and SAMtools. Bioinformatics *25*, 2078–2079.

Lindner, S.E., Swearingen, K.E., Harupa, A., Vaughan, A.M., Sinnis, P., Moritz, R.L., and Kappe, S.H. (2013). Total and putative surface proteomics of malaria parasite salivary gland sporozoites. Mol. Cell. Proteomics *12*, 1127–1143.

López-Barragán, M.J., Lemieux, J., Quiñones, M., Williamson, K.C., Molina-Cruz, A., Cui, K., Barillas-Mury, C., Zhao, K., and Su, X.Z. (2011). Directional gene expression and antisense transcripts in sexual and asexual stages of *Plasmodium falciparum*. BMC Genomics *12*, 587.

Lopez-Rubio, J.J., Siegel, T.N., and Scherf, A. (2012). Genome-wide chromatin immunoprecipitation-sequencing in Plasmodium. In Malaria: Methods and Protocols, R. Ménard, ed. (Humana Press), pp. 321–333.

Lorestani, A., Sheiner, L., Yang, K., Robertson, S.D., Sahoo, N., Brooks, C.F., Ferguson, D.J., Striepen, B., and Gubbels, M.J. (2010). A *Toxoplasma* MORN1 null mutant undergoes repeated divisions but is defective in basal assembly, apicoplast division and cytokinesis. PLoS One *5*, e12302.

Modrzynska, K., Pfander, C., Chappell, L., Yu, L., Suarez, C., Dundas, K., Gomes, A.R., Goulding, D., Rayner, J.C., Choudhary, J., and Billker, O. (2017). A knockout screen of ApiAP2 genes reveals networks of interacting transcriptional regulators controlling the plasmodium life cycle. Cell Host Microbe *21*, 11–22.

Nguyen Ba, A.N., Pogoutse, A., Provart, N., and Moses, A.M. (2009). NLStradamus: a simple Hidden Markov Model for nuclear localization signal prediction. BMC Bioinformatics *10*, 202.

Oehring, S.C., Woodcroft, B.J., Moes, S., Wetzel, J., Dietz, O., Pulfer, A., Dekiwadia, C., Maeser, P., Flueck, C., Witmer, K., et al. (2012). Organellar proteomics reveals hundreds of novel nuclear proteins in the malaria parasite *Plasmodium falciparum*. Genome Biol. *13*, R108.

Pachebat, J.A., Ling, I.T., Grainger, M., Trucco, C., Howell, S., Fernandez-Reyes, D., Gunaratne, R., and Holder, A.A. (2001). The 22 kDa component of the protein complex on the surface of *Plasmodium falciparum* merozoites is derived from a larger precursor, merozoite surface protein 7. Mol. Biochem. Parasitol. *117*, 83–89.

Painter, H.J., Campbell, T.L., and Llinás, M. (2011). The Apicomplexan AP2 family: integral factors regulating *Plasmodium* development. Mol. Biochem. Parasitol. *176*, 1–7.

Painter, H.J., Altenhofen, L.M., Kafsack, B.F., and Llinás, M. (2013). Whole-genome analysis of *Plasmodium spp*. Utilizing a new agilent technologies DNA microarray platform. Methods Mol. Biol. *923*, 213–219.

Proellocks, N.I., Coppel, R.L., and Waller, K.L. (2010). Dissecting the apicomplexan rhoptry neck proteins. Trends Parasitol. *26*, 297–304.

Quinlan, A.R., and Hall, I.M. (2010). BEDTools: a flexible suite of utilities for comparing genomic features. Bioinformatics *26*, 841–842.

Ramírez, F., Dündar, F., Diehl, S., Grüning, B.A., and Manke, T. (2014). deepTools: a flexible platform for exploring deep-sequencing data. Nucleic Acids Res. *42*, W187–W191.

Reilly, H.B., Wang, H., Steuter, J.A., Marx, A.M., and Ferdig, M.T. (2007). Quantitative dissection of clone-specific growth rates in cultured malaria parasites. Int. J. Parasitol. *37*, 1599–1607.

Richard, D., Kats, L.M., Langer, C., Black, C.G., Mitri, K., Boddey, J.A., Cowman, A.F., and Coppel, R.L. (2009). Identification of rhoptry trafficking determinants and evidence for a novel sorting mechanism in the malaria parasite *Plasmodium falciparum*. PLoS Pathog. *5*, e1000328.

Russell, K., Emes, R., and Horrocks, P. (2015). Triaging informative cis-regulatory elements for the combinatorial control of temporal gene expression during *Plasmodium falciparum* intraerythrocytic development. Parasit. Vectors *8*, 81.

Russo, I., Oksman, A., and Goldberg, D.E. (2009). Fatty acid acylation regulates trafficking of the unusual *Plasmodium falciparum* calpain to the nucleolus. Mol. Microbiol. *72*, 229–245.

Sanders, P.R., Kats, L.M., Drew, D.R., O'Donnell, R.A., O'Neill, M., Maier, A.G., Coppel, R.L., and Crabb, B.S. (2006). A set of glycosylphosphatidyl inositol-anchored membrane proteins of *Plasmodium falciparum* is refractory to genetic deletion. Infect. Immun. *74*, 4330–4338.

Sangurdekar, D.P. (2014). Rnits: R Normalization and Inference of Time Series data. R package version 1.4.0 (Bioconductor).

Schultz, J., Milpetz, F., Bork, P., and Ponting, C.P. (1998). SMART, a simple modular architecture research tool: identification of signaling domains. Proc. Natl. Acad. Sci. USA *95*, 5857–5864.

Sherling, E.S., Knuepfer, E., Brzostowski, J.A., Miller, L.H., Blackman, M.J., and van Ooij, C. (2017). The *Plasmodium falciparum* rhoptry protein RhopH3 plays essential roles in host cell invasion and nutrient uptake. Elife *6*, 6.

Shi, J., and Vakoc, C.R. (2014). The mechanisms behind the therapeutic activity of BET bromodomain inhibition. Mol. Cell *54*, 728–736.

Singh, S., and Chitnis, C.E. (2012). Signalling mechanisms involved in apical organelle discharge during host cell invasion by apicomplexan parasites. Microbes Infect. *14*, 820–824.

Sinha, A., Hughes, K.R., Modrzynska, K.K., Otto, T.D., Pfander, C., Dickens, N.J., Religa, A.A., Bushell, E., Graham, A.L., Cameron, R., et al. (2014). A cascade of DNA-binding proteins for sexual commitment and development in *Plasmodium*. Nature *507*, 253–257.

Spielmann, T., Fergusen, D.J., and Beck, H.P. (2003). *etramps*, a new *Plasmodium falciparum* gene family coding for developmentally regulated and highly charged membrane proteins located at the parasite-host cell interface. Mol. Biol. Cell *14*, 1529–1544.

Spycher, C., Rug, M., Pachlatko, E., Hanssen, E., Ferguson, D., Cowman, A.F., Tilley, L., and Beck, H.P. (2008). The Maurer's cleft protein MAHRP1 is essential for trafficking of PfEMP1 to the surface of *Plasmodium falciparum*-infected erythrocytes. Mol. Microbiol. *68*, 1300–1314.

Striepen, B., Jordan, C.N., Reiff, S., and van Dooren, G.G. (2007). Building the perfect parasite: cell division in apicomplexa. PLoS Pathog. *3*, e78.

Suvorova, E.S., Francia, M., Striepen, B., and White, M.W. (2015). A novel bipartite centrosome coordinates the apicomplexan cell cycle. PLoS Biol. *13*, e1002093.

Templeton, T.J., Iyer, L.M., Anantharaman, V., Enomoto, S., Abrahante, J.E., Subramanian, G.M., Hoffman, S.L., Abrahamsen, M.S., and Aravind, L. (2004). Comparative analysis of apicomplexa and genomic diversity in eukaryotes. Genome Res. *14*, 1686–1695.

Tham, W.H., Healer, J., and Cowman, A.F. (2012). Erythrocyte and reticulocyte binding-like proteins of *Plasmodium falciparum*. Trends Parasitol. *28*, 23–30.

Thorvaldsdóttir, H., Robinson, J.T., and Mesirov, J.P. (2013). Integrative Genomics Viewer (IGV): high-performance genomics data visualization and exploration. Brief. Bioinform. *14*, 178–192.

Trager, W., and Jensen, J.B. (1976). Human malaria parasites in continuous culture. Science *193*, 673–675.

Trucco, C., Fernandez-Reyes, D., Howell, S., Stafford, W.H., Scott-Finnigan, T.J., Grainger, M., Ogun, S.A., Taylor, W.R., and Holder, A.A. (2001). The merozoite surface protein 6 gene codes for a 36 kDa protein associated with the *Plasmodium falciparum* merozoite surface protein-1 complex. Mol. Biochem. Parasitol. *112*, 91–101.

Volz, J., Carvalho, T.G., Ralph, S.A., Gilson, P., Thompson, J., Tonkin, C.J., Langer, C., Crabb, B.S., and Cowman, A.F. (2010). Potential epigenetic regulatory proteins localise to distinct nuclear sub-compartments in *Plasmodium falciparum*. Int. J. Parasitol. *40*, 109–121.

Walker, D.M., Oghumu, S., Gupta, G., McGwire, B.S., Drew, M.E., and Satoskar, A.R. (2014). Mechanisms of cellular invasion by intracellular parasites. Cell. Mol. Life Sci. *71*, 1245–1263.

Weiss, G.E., Gilson, P.R., Taechalertpaisarn, T., Tham, W.H., de Jong, N.W., Harvey, K.L., Fowkes, F.J., Barlow, P.N., Rayner, J.C., Wright, G.J., et al. (2015). Revealing the sequence and resulting cellular morphology of receptor-ligand interactions during *Plasmodium falciparum* invasion of erythrocytes. PLoS Pathog. *11*, e1004670.

Wiśniewski, J.R., Zougman, A., and Mann, M. (2009). Combination of FASP and StageTip-based fractionation allows in-depth analysis of the hippocampal membrane proteome. J. Proteome Res. *8*, 5674–5678.

Wright, G.J., and Rayner, J.C. (2014). *Plasmodium falciparum* erythrocyte invasion: combining function with immune evasion. PLoS Pathog. *10*, e1003943.

Young, J.A., Johnson, J.R., Benner, C., Yan, S.F., Chen, K., Le Roch, K.G., Zhou, Y., and Winzeler, E.A. (2008). In silico discovery of transcription regulatory elements in *Plasmodium falciparum*. BMC Genomics *9*, 70.

Zhang, Y., Liu, T., Meyer, C.A., Eeckhoute, J., Johnson, D.S., Bernstein, B.E., Nusbaum, C., Myers, R.M., Brown, M., Li, W., and Liu, X.S. (2008). Model-based analysis of ChIP-Seq (MACS). Genome Biol. *9*, R137.

Zhang, Q., Huang, Y., Zhang, Y., Fang, X., Claes, A., Duchateau, M., Namane, A., Lopez-Rubio, J.J., Pan, W., and Scherf, A. (2011). A critical role of perinuclear filamentous actin in spatial repositioning and mutually exclusive expression of virulence genes in malaria parasites. Cell Host Microbe *10*, 451–463.

STAR★METHODS

KEY RESOURCES TABLE

REAGENT or RESOURCE	SOURCE	IDENTIFIER
Antibodies		
Rabbit anti-GFP	PI: Ileana Cristea Cristea et al., 2005	N/A
Mouse anti-GFP	Roche	Cat# 11814460001; RRID: AB_390913
Mouse anti-Histone H3	Abcam	Cat#ab10799; RRID: AB_470239
Rabbit anti-aldolase	Abcam	Cat#ab38905; RRID: AB_771788
Rat anti-HA high-affinity 3F10	Roche	Cat#11867423001; RRID: AB_10094468
Rabbit anti-GFP	Abcam	Cat#ab290; RRID: AB_303395
Rabbit anti-IgG	Abcam	Cat#ab46540; RRID: AB_2614925
Rabbit anti-MSP4	Malaria Research and Reference Reagent Resource Center	Cat#MRA-319
Rabbit anti-MSP5	Malaria Research and Reference Reagent Resource Center	Cat#MRA-320
Alexa 488 conjugated anti-GST antibody	Thermo Fisher Scientific	Cat#A-11131; RRID: AB_2534137
Goat anti-mouse IgG HRP-conjugate	Pierce Thermo Fisher Scientific	Cat#31437; RRID: AB_228295
Goat anti-rabbit IgG HRP-conjugate	Millipore	Cat#12-348; RRID: AB_390191
Goat anti-rat IgG HRP-conjugate	Millipore	Cat#AB136P
Bacterial and Virus Strains		
DH5α pB-3′*pfap2-i*-GFP	This manuscript	N/A
DH5α pJDD-5′*bdp1*	This manuscript	N/A
DH5α pDC2-cam-PfAP2-I_{NLS}-GFP	This manuscript	N/A
DH5α pDC2-CAM-PfSIP2$_{NLS}$-GFP	This manuscript	N/A
DH5α pL7-*msp5*MUT-gRNA*msp5*	This manuscript	N/A
DH5α pL7-D1MUT-gRNAD1	This manuscript	N/A
DH5α pL7-D2MUT-gRNAD2	This manuscript	N/A
DH5α pL7-D3MUT-gRNAD3	This manuscript	N/A
BL21-CodonPlus(DE3)-RIL pGEX-D1-GST	PI: Manuel Llinás Campbell et al., 2010	N/A
BL21-CodonPlus(DE3)-RIL pGEX-D2-GST	PI: Manuel Llinás Campbell et al., 2010	N/A
DH5α pGEX-D1mut-GST	This manuscript	N/A
BL21-CodonPlus(DE3)-RIL pGEX-D1mut-GST	This manuscript	N/A
DH5α pGEX-D2mut-GST	This manuscript	N/A
BL21-CodonPlus(DE3)-RIL pGEX-D2mut-GST	This manuscript	N/A
DH5α pGEX-D3mut-GST	This manuscript	N/A
BL21-CodonPlus(DE3)-RIL pGEX-D3mut-GST	This manuscript	N/A
BL21-CodonPlus(DE3)-RIL	Agilent Technologies	Cat#230240
DH5α	Thermo Fisher Scientific	Cat#18265017

(*Continued on next page*)

Continued

REAGENT or RESOURCE	SOURCE	IDENTIFIER
Chemicals, Peptides, and Recombinant Proteins		
Blasticidin-S-HCl	Thermo Fisher Scientific	Cat#R21001
WR99210	Jacobus Pharmaceuticals	N/A
DSM1	Malaria Research and Reference Reagent Resource Center	Cat#MRA1161
Shld-1	Clontech (Takara)	Cat#632188
KAPA HiFi PCR kit	KAPA Biosystems	Cat#KK2101
NEBNext DNA library Prep	NEB	Cat#E6000S
Power SYBR Green master mix	Thermo Fisher Scientific	Cat#4367659
SuperScript II Reverse Transcriptase	Thermo Fisher Scientific	Cat#18064022
Hoechst 33342	Life Technologies	Cat#H3570
Coomassie Brilliant Blue	Thermo Fisher Scientific	Cat#20278
TRIzol	Thermo Fisher Scientific	Cat#10296010
Amersham CyDye Reactive Dyes	GE Healthcare	Cat#RPN5661
IPTG	Sigma	Cat#10724815001
Critical Commercial Assays		
Qubit dsDNA HS Assay Kit	Thermo Fisher Scientific	Cat#Q32851
DNeasy Blood & Tissue kit	QIAGEN	Cat#69504
In-Fusion HD Cloning Plus	Clontech (Takara)	Cat#638909
ECL western blotting substrate	Pierce	Cat#32132
MinElute PCR purification kit	QIAGEN	Cat#28004
DNA Clean and Concentrator-5 kit	Zymo Research	Cat#D4004
Deposited Data		
Dd2 draft genome	Sanger Institute	ftp://ftp.sanger.ac.uk/pub/pathogens/Plasmodium/falciparum/PF3K/PilotReferenceGenomes/DraftAnnotation/PfDd2/
PfBDP1-HA ChIP-seq data	Josling et al., 2015	GEO: GSE79135
PfAP2-I-GFP ChIP-seq data	This manuscript	GEO: GSE80293
PfAP2-I-GFP and PfAP2-I-GFP::*msp5*MUT DNA microarray data	This manuscript	GEO: GSE77807, GSE77810
Protein-binding microarray data	This manuscript	UniPROBE: UP01415 UniPROBE Database: http://uniprobe.org/
PfAP2-I-GFP immunoaffinity purification data	This manuscript	Table S4
Protein-binding microarray position weight matrices	This manuscript	Table S6
Experimental Models: Cell Lines		
P. falciparum: 3D7	Malaria Research and Reference Reagent Resource Center	Cat#MRA-102
P. falciparum: Dd2	Malaria Research and Reference Reagent Resource Center	Cat#MRA-150
Experimental Models: Organisms/Strains		
PfCHD1-GFP	PI: Alan Cowman Volz et al., 2010	N/A
PfAP2-I-GFP	This manuscript	N/A
PfAP2-I-GFP::*msp5*MUT	This manuscript	N/A
PfAP2-I-GFP-D1mut	This manuscript	N/A
PfAP2-I-GFP-D2mut	This manuscript	N/A
PfAP2-I_{NLS}-GFP	This manuscript	N/A
PfAP2-I-GFP::PfBDP1-HA-DD	This manuscript	N/A
NLS_{PfSIP2}-GFP	This manuscript	N/A

(*Continued on next page*)

Continued

REAGENT or RESOURCE	SOURCE	IDENTIFIER
$NLS_{Calmodulin}$-YFP	PI: Daniel Goldberg Russo et al., 2009	N/A
PfSIP2N-HA	PI: Till Voss Flueck et al., 2009	N/A
HDGFP	PI: Kasturi Haldar Kadekoppala et al., 2000	N/A
Oligonucleotides		
NEXTflex Illumina DNA barcodes	Bioo Scientific 514103	Cat#514103
Primers listed in Table S1	Integrated DNA Technologies	http://www.idtdna.com/site
Random nonamers and oligo(dT) primers	Integrated DNA Technologies	http://www.idtdna.com/site
Recombinant DNA		
pBcam-3xHA plasmid	PI: Till Voss Flueck et al., 2009	N/A
pJDD41 plasmid	PI: Manoj Duraisingh Dvorin et al., 2010	N/A
pL6-CS plasmid	PI: Jose-Juan Lopez-Rubio Ghorbal et al., 2014	N/A
pDC2-cam-CRT-GFP plasmid	PI: Thomas E. Wellems Fidock et al., 2000	N/A
D3MUT sequence	Genewiz	N/A
pGEX-4T1 plasmid	GE Life Sciences	Cat#28-9545-49
PhiX control DNA v3	Illumina	Cat#FC-110-3001
Software and Algorithms		
FastQC v.0.11.2	Andrew, 2010	http://www.bioinformatics.babraham.ac.uk/projects/fastqc/
Trimmomatic	Bolger et al., 2014	http://www.usadellab.org/cms/?page=trimmomatic
BWA MEM	Li, 2013	http://bio-bwa.sourceforge.net/
SAMtools	Li et al., 2009	http://samtools.sourceforge.net/
MACS2 v.2.1.1.20160309	Zhang et al., 2008	https://github.com/taoliu/MACS
DREME	Bailey, 2011	http://meme-suite.org/tools/dreme
FIMO	Grant et al., 2011	http://meme-suite.org/tools/fimo
TOMTOM	Gupta et al., 2007	http://meme-suite.org/tools/tomtom
BEDTools suite	Quinlan and Hall, 2010	http://bedtools.readthedocs.io/en/latest/
pybedtools	Dale et al., 2011	https://daler.github.io/pybedtools/
deepTools	Ramírez et al., 2014	https://deeptools.github.io/
seqLogo	Bembom, 2017	http://bioconductor.org/packages/release/bioc/html/seqLogo.html
Integrated Genomics Viewer	Thorvaldsdóttir et al., 2013	http://software.broadinstitute.org/software/igv/
ImageLab software of ChemiDoc MP Imaging System	Bio-Rad	N/A
SMART	Letunic et al., 2012; Schultz et al., 1998	http://smart.embl-heidelberg.de/
NLStradamus	Nguyen Ba et al., 2009	http://www.moseslab.csb.utoronto.ca/NLStradamus/
Multalin	Corpet, 1988	http://multalin.toulouse.inra.fr/multalin/
Proteome Discoverer	Thermo Scientific	N/A
SEQUEST	Eng et al., 1994	N/A
Rnits	Sangurdekar, 2014	N/A
SAINT	Choi et al., 2011	http://saint-apms.sourceforge.net/Main.html
PBM analysis suite	Berger and Bulyk, 2009	http://the_brain.bwh.harvard.edu/PBMAnalysisSuite/index.html

(*Continued on next page*)

Continued

REAGENT or RESOURCE	SOURCE	IDENTIFIER
Other		
Dynabeads M-270 Epoxy	Thermo Fisher Scientific	Cat#14301
Magna ChIP protein A+G magnetic beads	Millipore	Cat#16-663
Agencourt AMPure XP beads	Beckman Coulter	Cat#A63880
Advantage Genomic LA Polymerase Mix	Clontech (Takara)	Cat#639153

CONTACT FOR REAGENT AND RESOURCE SHARING

Further information and requests for resources and reagents should be directed to and will be fulfilled by the Lead Contact, Manuel Llinás (manuel@psu.edu).

EXPERIMENTAL MODEL AND SUBJECT DETAILS

Parasite Culture and Transfection

P. falciparum parasites were cultured at 37C in the presence of 5% oxygen and 7% carbon dioxide, in RPMI 1640 media supplemented with hypoxanthine and 0.5% Albumax II (Invitrogen) (culture media recipe can be found at http://llinaslab.psu.edu/protocols/) in 2% or 5% haemotocrit. Parasites were fed fresh blood every other day and parasitemia was kept at around 2%–5% by counting the number of parasites in blood smears (Trager and Jensen, 1976).

Parasite synchronization to the ring stage was done by incubating pelleted cultures 1:1 with 0.3M L-Alanine, 10mM HEPES pH 7.5 solution for 10 min at 37C, after which cultures were centrifuged, resuspended in fresh media and placed back in culture (Braun-Breton et al., 1988). All experiments, unless stated otherwise, were performed at 40h post-invasion.

When necessary to induce a knockdown, DD-FKBP parasites were synchronized and Shld-1 was removed for 26h.

Parasite Strains

Dd2	wt strain	grown in standard culture media
PfAP2-I-GFP	Dd2 strain with endogenous PfAP2-I C-terminally tagged with GFP	grown in standard media supplemented with BSD
PfSIP2N-HA	3D7 strain expressing episomal copy of PfSIP2 N terminus fused to 3xHA	grown in standard media supplemented with BSD; Flueck et al., 2009
PfAP2-I-GFP::msp5MUT	PfAP2-I-GFP Dd2 strain with mutated PfAP2-I DNA motif in the promoter of endogenous *msp5*	grown in standard media
PfAP2-I-GFP-D1mut	PfAP2-I-GFP Dd2 strain with mutated AP2 domain 1 (D1)	grown in standard media
PfAP2-I-GFP-D2mut	PfAP2-I-GFP Dd2 strain with mutated AP2 domain 2 (D2)	grown in standard media
PfAP2-INLS-GFP	Dd2 strain expressing episomal copy of $NLS_{PfAP2\text{-}I}$-GFP	grown in standard media supplemented with WR
NLSPfSIP2-GFP	Dd2 strain expressing episomal copy of NLS_{PfSIP2}-GFP	grown in standard media supplemented with WR
NLSCalmodulin-YFP	3D7 strain expressing episomal copy of $NLS_{Calmodulin}$-YFP	grown in standard media supplemented with WR; Russo et al., 2009
HDGFP	3D7 strain expressing cytosolic GFP	grown in standard media supplemented with WR; Kadekoppala et al., 2000
PfAP2-I-GFP::PfBDP1-HA-DD	PfAP2-I-GFP Dd2 strain with endogenous PfBDP1 C-terminally tagged with 3xHA and FKBP (DD)	grown in standard media supplemented with WR and BSD
PfCHD1-GFP	3D7 strain with endogenous PfCHD1 C-terminally tagged with GFP	grown in Standard media supplemented with WR; Volz et al., 2010

All parasite strains are available upon request.

Bacterial Strains

pB-3′pfap2-i-GFP	DH5α bacterial strain carrying pB-3′*pfap2-i*-GFP
pJDD-3′bdp1	DH5α bacterial strain carrying pJDD-3′*bdp1*
pDC2-cam-PfAP2-INLS-GFP	DH5α bacterial strain carrying pDC2-cam-PfAP2-I_{NLS}-GFP
pDC2-CAM-PfSIP2NLS-GFP	DH5α bacterial strain carrying pDC2-CAM-PfSIP2$_{NLS}$-GFP
pL7-msp5MUT-gRNAmsp5	DH5α bacterial strain carrying pL7-*msp5*MUT-gRNA*msp5*
pL7-D1MUT-gRNAD1	DH5α bacterial strain carrying pL7-D1MUT-gRNAD1
pL7-D2MUT-gRNAD2	DH5α bacterial strain carrying pL7-D2MUT-gRNAD2
pL7-D3MUT-gRNAD3	DH5α bacterial strain carrying pL7-D3MUT-gRNAD3
pGEX-D1-GST	BL21 bacterial strain carrying pGEX-D1-GST (previously generated)
pGEX-D2-GST	BL21 bacterial strain carrying pGEX-D2-GST (previously generated)
pGEX-D1mut-GST	DH5α bacterial strain carrying pGEX-D1mut-GST
pGEX-D1mut-GST(BL21)	BL21 bacterial strain carrying pGEX-D1mut-GST
pGEX-D2mut-GST	DH5α bacterial strain carrying pGEX-D2mut-GST
pGEX-D2mut-GST(BL21)	BL21 bacterial strain carrying pGEX-D2mut-GST
pGEX-D3mut-GST	DH5α bacterial strain carrying pGEX-D3mut-GST
pGEX-D3mut-GST(BL21)	BL21 bacterial strain carrying pGEX-D3mut-GST

All DH5α strains were grown in LB media supplemented with Ampicillin and all BL21-CodonPlus(DE3)-RIL cells (BL21) strains were grown in LB media supplemented with chloramphenicol. All bacterial strains are available as glycerol stocks upon request.

METHOD DETAILS

P. falciparum Transfections

Plasmid transfections into *P. falciparum* parasites were performed by electroporation using a Gene-Pulser II (Bio-Rad) as previously described (Fidock and Wellems, 1997). Briefly, ring-stage parasites at 5% haemotocrit were washed 3 times with warm cytomix (120 mM KCl, 0.2 mM $CaCl_2$, 2 mM EGTA, 10 mM $MgCl_2$, 25 mM HEPES, 5 mM K_2HPO_4, 5 mM KH_2PO_4; pH 7.6) and resuspended to 50% haemotocrit with ice-cold cytomix. Parasites were then electroporated with 100μg of plasmid DNA resuspended in cytomix. All CRISPR/Cas9 parasite lines were generated by co-transfecting parasites with 30μg of pL7 plasmid and 30μg of the pUF1-Cas9 plasmid (Ghorbal et al., 2014). Transfected parasites were resuspended in warm media and cultured overnight in complete media plus 2% hematocrit. The next day, transfectants were selected on either 2μg/ml blasticidin-S-HCl (BSD) and/or 2.5nM WR99210 (WR) and/or 1.5μM 5-methyl[1,2,4]triazolo[1,5-a]pyrimidin-7-yl)naphthalen-2-ylamine (DSM1). PfAP2-I-GFP::PfBDP1-HA-DD parasites were generated by growing parasites in the presence of 0.5μM Shld-1 (Takara). When PfAP2-I-GFP Dd2 parasites were used for transfection, the media was supplemented with BSD. When necessary, parasites were cycled ON/OFF drugs for at least 2 cycles and cloned by serial dilution in order to ensure that the population was clonal for plasmid integration. Transfected lines were verified by PCR using genomic DNA collected with a DNeasy Blood & Tissue kit (QIAGEN, RRID: SCR_008539) and using the appropriate primers and by Western-blot. Parasite lines generated using CRISPR/Cas9 had the locus of interest sequenced by Sanger sequencing.

Antibodies

The primary antibodies used were: mouse anti-GFP 11814460001 (Roche, RRID: AB_390913) (Western-blot, 1:1000 dilution), in-house developed rabbit anti-GFP (Cristea et al., 2005) (immunoaffinity purification), mouse anti-Histone H3 10799 (Abcam, RRID: AB_470239) (Western-blot, 1:2000 dilution), rabbit anti-aldolase 38905 (Abcam, RRID: AB_771788) (Western-blot, 1:1000 dilution), rat anti-HA high affinity 3F10 (Roche, RRID: AB_10094468) (Western blot: 1/200 dilution and ChIP), rabbit anti-GFP 290 (Abcam, RRID: AB_303395) (ChIP), rabbit anti-IgG 46540 (Abcam, RRID: AB_2614925) (ChIP and immunoaffinity purification), rabbit anti-MSP4 MRA-319 (MR4) (Western-blot, 1:1000 dilution), and rabbit anti-MSP5 MRA-320 (MR4) (Western-blot, 1:1000 dilution),. Secondary antibodies used were: goat anti-mouse IgG (Fc) peroxidase conjugated (ThermoFisher Scientific), goat anti-rabbit IgG HRP-conjugate (Millipore, RRID: AB_390191) and goat anti-rat IgG HRP-conjugate (Millipore, RRID: AB_11214444) at 1:3000 dilutions. Hoechst 33342 (Life Technologies) was used in all live immunofluorescence assays to visualize the nucleus. For details on the concentration of antibodies used for ChIP or immunoaffinity purification refer to those protocols below.

Plasmid DNA Cloning

All primers used for cloning are listed in Table S1.

Restriction enzymes were purchased from New England Biolabs (NEB, RRID: SCR_013517).

All PCRs were performed using Advantage Genomic LA Polymerase Mix (Clontech) according to the manufacturer's instructions.

In order to tag *pf3d7_1007700* (*pfap2-i*) with GFP, 1040bp from the 3′end of the gene were amplified from 3D7 genomic DNA with primers AP2-I-1 and AP2-I-2 (Table S1) and cloned into the pBcam-GFP plasmid between BglII and *NotI*, generating pB-3′*pfap2-i*-GFP. The plasmid pBcam-GFP was generated by amplifying the GFP sequence with primers GFP-1 and GFP-2 and cloning into the pBcam-3xHA plasmid (Flueck et al., 2009) between *NotI* and SalI.

To endogenously tag *pfbdp1* with 3xHA-DD-FKBP in PfAP2-I-GFP parasites, 1383bp of the 3′end of the gene was amplified from 3D7 genomic DNA with primers BDP1-1 and BDP1-2 and cloned into the pJDD41 plasmid (Dvorin et al., 2010) between *NotI* and *XhoI*, generating pJDD41-3′*bdp1*.

In order to express the putative NLS of PfAP2-I or PfSIP2 fused to GFP, primers NLS2-1 and NLS2-2 or SIP2-1 and SIP2-2 were used to amplify the NLS sequences and the PCR products were cloned into the pDC2-cam-CRT-GFP plasmid (Fidock et al., 2000) between *AvrII* and *SpeI*, generating pDC2-cam-PfAP2-I_{NLS}-GFP and pDC2-CAM-PfSIP2$_{NLS}$-GFP, respectively.

The ATGCA DNA motif upstream of *msp5* was mutated in PfAP2-I-GFP parasites using the plasmid pL6-*msp5*MUT-gRNA*msp5*, which was generated by cloning the guide RNA created by annealing the primers gRNA MSP5-1 and gRNA MSP5-2 and cloning the annealed product into the pL6-CS plasmid (Ghorbal et al., 2014) into the *BtgZI* site using In-Fusion HD Cloning Plus (Clontech) according to the manufacturer's instructions.

The *msp5*MUT sequence was generated by amplifying two mutated arms with primers MSP5-1 and MSP5-2 and primers MSP5-3 and MSP5-4, then ligating with In-Fusion (primers MSP5-2 and MSP5-3 have 15bp homology with each other) and re-amplifying the ligated product with primers MSP5-1 and MSP5-4 (Table S1). The final mutated product was cloned with In-Fusion into the pL6-gRNA*msp5* plasmid between *NotI* and *SpeI* (primers MSP5-1 and MSP5-4 have 15bp homology to the pL6-CS plasmid), generating pL7-*msp5*MUT-gRNA*msp5*. The plasmids used to mutate the first, second and third AP2 domains of PfAP2-I in PfAP2-I-GFP parasites were created by cloning the guide RNA created by annealing the primers gRNA D1-1 and gRNA D1-2 or gRNA D2-1 and gRNA D2-2 or gRNA D3-1 and gRNA D3-2, respectively, and cloning the annealed products In-Fusion into the pL6-CS plasmid in the *BtgZI* site, according to the manufacturer's instructions. The D1MUT and D2MUT sequences were generated by amplifying mutated arms with primers D1-1 and D1-2 and primers D1-3 and D1-4 or with primers D2-1 and D2-2 and primers D2-3 and D2-4 (Table S1), then ligating with In-Fusion and re-amplifying the ligated product with primers D1-1 and D1-4 or D2-1 and D2-4. The final mutated products were cloned into the pL6-gRNAD1 or pL6-gRNAD2 plasmids between *NotI* and *SpeI*, generating pL7-D1MUT-gRNAD1 and pL7-D2MUT-gRNAD2, respectively. The D3MUT sequence (2727-3100bp *pfap2-I* ORF) was gene synthesized by Genewiz (RRID: SCR_003177) (Table S1) and cloned into pL7-gRNAD3 between Not I and SpeI, generating pL7-D3MUT-gRNAD3.

DNA sequences encoding for the AT-hook alone (AT) or the AT-hook fused to the second AP2 domain (AT-D2) were PCR amplified from 3D7 gDNA using primers AT-1 and AT-2 or AT-1 and D2-5, respectively, and cloned into the BamHI and *XhoI* sites in the pGEX-4T1 plasmid (GE Life Sciences, RRID: SCR_000004) to create the N-terminal glutathione S-transferase (GST) fusions pGEX-AT-GST and pGEX-AT-D2-GST. DNA sequences encoding mutant versions of the first (D1), second (D2) or third (D3) AP2 domains were PCR amplified from pL7-D1MUT-gRNAD1, pL7-D2MUT-gRNAD2 or pL7-D3MUT-gRNAD3 using primers D1-4 and D1-5 or D2-6 and D2-7 or D3-1 and D3-2, respectively, and cloned into the BamHI and *XhoI* sites in the pGEX-4T1 plasmid to create the N-terminal glutathione S-transferase (GST) fusions pGEX-D1mut-GST, pGEX-D2mut-GST and pGEX-D3mut-GST.

All plasmids were verified by Sanger-sequencing and diagnostic restriction digestion.

Expression and Purification of Recombinant Proteins

GST-tagged recombinant proteins were expressed in BL21-CodonPlus(DE3)-RIL cells (Agilent Technologies) by inducing with 0.2mM IPTG at room temperature overnight, and were affinity purified using glutathione resin (Clontech) (protocol can be found at http://llinaslab.psu.edu/protocols/). The efficiency of the purification was estimated by Coomassie blue staining. GST-D1 proteins could not be purified and the bacterial lysate was used instead for protein binding microarrays.

Protein Binding Microarrays

Bacterial lysate or purified recombinant proteins were assayed for DNA binding as previously described in (Campbell et al., 2010) using protein binding microarrays (PBMs). Briefly, custom designed DNA oligonucleotide arrays were double-stranded using a universal primer, incubated with GST-AP2 fusion proteins, visualized with Alexa 488 conjugated anti-GST antibody (Millipore, RRID: AB_2534137), and scanned using an Axon 4200A scanner. Proteins were used at the maximum concentration obtained from purification and represent one-fifth of the total reaction volume used on the PBM. After data normalization and calculation of enrichment scores the ''Seed-and-Wobble'' algorithm was applied to combine the data from two separate experiments and create position weight matrices (PWMs).

As a control, PBMs were performed with the lysate of GST-D1 expressing cells or newly purified GST-D2 protein previously used in (Campbell et al., 2010). Each GST-tagged protein was run on two PBM array versions, AMADID 016060 (v9) and AMADID 015681 (v11), with the exception of GST-AT which was only tested on v9. DNA binding motifs from the two arrays were combined to generate the final binding motif reported.

Bioinformatic Searches

Simple Modular Architecture Research Tool (SMART) (Letunic et al., 2012; Schultz et al., 1998) was used to predict the AT-hook motif in the PfAP2-I sequence. NLS were predicted using NLStradamus (Nguyen Ba et al., 2009). Multalin (Corpet, 1988) was used for the protein sequence alignments shown throughout.

Nuclear Fractionation Assays and Western Blot

Nuclear fractionation assays were performed as previously described (Flueck et al., 2010). Briefly, saponin-lysed infected red blood cells were lysed in ice-cold cell lysis buffer (20mM HEPES pH 7.9, 10mM KCl, 1mM EDTA, 1mM EGTA, 1mM DTT, protease inhibitors) for 5 min. After a 5 min centrifugation at 5200 rpm (2500xg), the cytosolic extract was collected and the cell pellet was re-suspended in ice-cold nuclear extraction buffer (20mM HEPES pH 7.9, 1M KCl, 1mM EDTA, 1mM EGTA, 1mM DTT, protease inhibitors). After a 30 min incubation at 4C, the mixture was centrifuged at 11800 rpm (13000xg) for 30 min and the nuclear extract collected (protocol can be found at http://llinaslab.psu.edu/protocols/). The cytosolic and nuclear extracts were diluted in SDS-polyacrylamide gel electrophoresis (SDS-PAGE) loading buffer containing 100mM DTT and boiled for 10 min before running in a SDS-PAGE gel. SDS-PAGE was performed using standard methods. Separated proteins were transferred to a nitrocellulose membrane and western blots were performed using primary antibodies diluted in 5% non-fat milk powder in 1X PBS-0.05% Tween. As a secondary antibody, a peroxidase-conjugated goat anti-mouse/rabbit/rat antibody was used. Bound antibodies were visualized using an established ECL western blotting substrate (Pierce).

Immunoaffinity Purification Assays

High salt nuclear extracts from PfAP2-I-GFP parasites were prepared as described above for the nuclear fractionation assays. The cytosolic and nuclear extracts were then diluted 4 times in dilution buffer (20mM HEPES pH7.9, 1mM EDTA, 1mM EGTA, 40% glycerol, protease inhibitors).

5mg M-270 Epoxy Dynabeads (ThermoFisher Scientific) were conjugated with 12.5μg of a custom polyclonal anti-GFP antibodies (Cristea et al., 2005) or 25μg IgG. Beads were twice washed in 0.1M sodium phosphate buffer (pH 7.4) and conjugated by incubating the beads with the antibody (20μl total volume per milligram of beads), 1M ammonium sulfate and 0.1M sodium phosphate overnight at 30C, while rotating the tubes. After extensive washing, the conjugated beads were stored at 4C in 1xPBS supplemented with 0.02% NaN_3 for up to one week (Joshi et al., 2013).

The diluted nuclear and cytosolic extracts were incubated with the conjugated beads as previously described in (Joshi et al., 2013) for 1.5h, at 4C. The beads were then extensively washed, and the protein complexes were eluted and digested in-solution with trypsin. The eluates were mixed with 8M Urea buffer in an ultra-filtration device and centrifuged 30min. The filters were then first washed once with 1M iodoacetamide and then three times with 0.01M ammonium bicarbonate. The washed filter units were transferred into a tube pre-washed with 200μl 50% acetonitrile, and the peptides were digested with 100 μl of 5ng/μl trypsin at 37C, overnight. The next day, the filter units were centrifuged and eluted twice with 50μl HPLC water. The elutions were transferred into an autosampler vial pre-loaded with 22μl of 10% trifluoroacetic acid and the samples were concentrated by vacuum centrifugation until the total volume was 10-30μl (Greco et al., 2012). The samples were then analyzed by mass spectrometry.

The immunoaffinity purification eluted material was digested using the filter aided sample preparation (FASP) protocol (Wiśniewski et al., 2009). Enzymatic digestion was performed in 100 mL of trypsin solution (5 ng/ml in 100mM ammonium bicarbonate) in Vivacon 500 centrifugal filters (10 kDa MWCO; Sartorius Stedim Biotech, Goettingen, Germany). Digested peptides were concentrated by vacuum centrifugation, desalted using StageTips constructed using Empore C_{18} extraction discs (3M Analytical Biotechnologies). Alternatively, the eluted material obtained from the immunopurification done with PfAP2-I-GFP parasites and GFP-conjugated beads underwent gel-assisted proteolysis, as described in (Han et al., 2008) (Table S4). Desalted peptides were analyzed by nanoliquid chromatography–tandem mass spectrometry using a Dionex Ultimate 3000 nRSLC coupled to an LTQ-Orbitrap Velos mass spectrometer (ThermoFisher Scientific, San Jose, CA), as described (Joshi et al., 2013). MS/MS spectra were extracted by Proteome Discoverer and analyzed using SEQUEST (Eng et al., 1994) by searching *P. falciparum* and contaminant protein databases.

As controls, extracts from parasites expressing GFP fused to nuclear localization signals (NLS) - NLS_{PfSIP2}-GFP (Figure S6A) or $NLS_{Calmodulin}$-YFP (Russo et al., 2009) – or expressing GFP in the cytosol – HDGFP (Kadekoppala et al., 2000) were also prepared (Figure S1C; Table S4). Each immunoaffinity purification was performed two independent times and only proteins that were detected in both replicates with 3 or more peptides were considered for further analysis.

DNA Microarrays

RNA from tightly synchronized PfAP2-I-GFP and PfAP2-I-GFP::*msp5*MUT parasites was harvested every 6h starting at 42h post-invasion for 24h (Figure S3G) and purified using a TRIzol (ThermoFisher Scientific) extraction method. The RNA was then reverse transcribed into cDNA using Superscript II RT (ThermoFisher) according to the manufacturer's instructions, and the cDNA was concentrated using DNA Clean and Concentrator-5 (Zymo Research) according to the manufacturer's instructions. The cDNA was labeled with CyDye (Cy5 sample, Cy3 reference pool) using Amersham CyDye Reactive Dyes (GE Healthcare) according to the manufacturer's instructions, and purified using DNA Clean and Concentrator-5 kit. DNA microarrays were performed as described in (Painter et al., 2013). RNA extraction, reverse transcription, cDNA labeling, array hybridization and washing protocols can be found at http://llinaslab.psu.edu/protocols/.

ChIP-Seq

The ChIP-seq assay was performed as described in (Lopez-Rubio et al., 2012) with some modifications. Synchronized 40h schizont stage parasite cultures were either formaldehyde-crosslinked and then lysed with saponin until complete red blood cell lysis (ChIP replicates 1 and 2), or saponin-lysed and then formaldehyde-crosslinked (ChIP replicate 3). The isolated chromatin was sheared in SDS lysis buffer to obtain a fragment size of 100-150bp using an M220 focused-ultrasonicator (Covaris Inc.) and the following settings: peak power 75W, 2% duty factor, 200 cycles per burst and total treatment time of 900 s. After pre-clearing the chromatin with Magna ChIP protein A+G magnetic beads (Millipore) (ChIP replicates 1 and 2) or protein A salmon sperm agarose beads (Millipore) (ChIP replicate 3), an input sample was collected and the rest of the chromatin was incubated overnight at 4C with 1 μg of polyclonal anti-GFP or, as control, the same amount of IgG. The immunoprecipitated chromatin was collected with A+G magnetic beads (ChIP replicates 1 and 2) or agarose beads (ChIP replicate 3), extensively washed and eluted with elution buffer. The input and ChIP samples were reverse cross-linked overnight at 45C in the presence of 0.4M NaCl and purified by phenol:chloroform or using the QIAGEN MinElute PCR purification kit.

Barcoded libraries for Illumina TruSeq single-end sequencing were constructed using NEBNext DNA library Prep reagents (New England Biolabs) by following the standard Illumina library preparation protocol. The DNA was first end-repaired for 30 min at 20C, purified using Agencourt AMPure XP beads (Beckman Coulter) (ChIP replicates 1 and 2) or via phenol:chloroform extraction (ChIP replicate 3) and then dA-tailed for 30 min at 37C, and purified using Ampure XP beads (ChIP replicates 1 and 2) or via phenol: chloroform extraction (ChIP replicate 3). NEXTflex Illumina DNA barcodes (diluted 1/10) were then ligated to the DNA fragments using T4 DNA ligase at 20C for 15 min. The resulting DNA was then size selected for 250 bp inserts using Ampure XP beads (ChIP replicates 1, 2 and 3). Afterward the libraries were PCR-amplified using Kapa HiFi (Kapa biosystems) and purified using AMPure XP beads. The quality and percentage of adaptor-ligated material of the final sequencing libraries was determined by running them on an Agilent 2100 Bioanalyzer (Agilent Technologies). The concentration of each library was determined using a Qubit dsDNA HS Assay kit (Invitrogen). The final libraries were multiplexed with three to fourteen barcoded samples and contained up to 20% PhiX control DNA per lane on an Illumina (RRID: SCR_010233) HiSeq 2500 system to generate 150 base pair single-end reads.

ChIP-qPCR

The primers used for ChIP-qPCR are listed in Table S1.

The ChIP-qPCR assays were performed as described for ChIP-Seq with few exceptions. The isolated chromatin was sheared in SDS lysis buffer to obtain a fragment size of 500bp using an M220 focused-ultrasonicator and the following settings: 10% duty factor, 200 cycles per burst and total treatment time of 60 s. After pre-clearing, an input sample was collected and the rest of the chromatin was incubated overnight at 4C with 1 μg of polyclonal anti-GFP/anti-HA antibody or, as control, the same amount of IgG. The immunoprecipitated chromatin was collected with Magna ChIP protein A+G magnetic beads (Millipore), extensively washed and eluted with elution buffer. The input and ChIP samples were reverse cross-linked overnight at 45C in the presence of 0.4M NaCl, and purified by phenol:chloroform extraction or using the QIAGEN MinElute PCR purification kit. For quantitative PCR (qPCR), the concentration of each eluted sample was determined by Qubit dsDNA Broad-Range Assay Kit (Invitrogen), diluted 10 times and used for quantitative PCR in triplicate wells using PowerSYBR Green Master Mix (ThermoFisher Scientific) as described (Crowley et al., 2011). Each ChIP-qPCR experiment was performed with at least 3 biological replicates.

For ChIP-qPCR from the PfAP2-I-GFP::PfBDP1-HA-DDline, parasites were grown ± Shld-1 for the times indicated and, after pre-clearing, an input sample was collected. The remainder of the chromatin was incubated overnight at 4C with 1 μg of polyclonal anti-GFP or anti-HA antibody. As a control, the same amount of IgG antibody was used.

RT-qPCR

cDNA was synthesized from approximately 2μg RNA using SuperScript II Reverse Transcriptase (ThermoFisher Scientific) with random nonamers and oligo(dT) primers according to the manufacturer's instructions. Controls containing all reaction components except SuperScript II were also set up to serve as no enzyme controls. qPCR was performed as described above. The list of primers used is in Table S1.

QUANTIFICATION AND STATISTICAL ANALYSIS

Western Blot Protein Quantification

Protein quantification was performed using the ImageLab software of ChemiDoc MP Imaging System (Bio-Rad).

Nuclear extraction efficiency was estimated using anti-histone H3 and anti-aldolase as nuclear and cytosolic markers, respectively.

ChIP-qPCR and RT-PCR Data Analysis

ChIP-qPCR and RT-PCR data were analyzed using the ΔΔCt method.

3D7 *wt* parasites or in the case of the parasite line PfAP2-I-GFP::PfBDP1-HA-DD, parasites treated without the ligand Shld-1, were used as controls.

pf3d7_0717700 (serine tRNA ligase) was used as a reference gene for RT-PCR.

In all figure legends, n denotes biological replicates (independently collected samples). Data are represented as mean ± SD.

DNA Microarrays

All sample data was compared to an arbitrary reference pool made-up of a mixed parasite population of rings, trophozoites and schizonts. The results shown represent the $\log_2$ ratio against the cDNA reference pool and are the average of 2 biological replicates.

Rnits (Sangurdekar, 2014) was used to determine a p value for all transcripts detected by DNA microarray (minus antigenic variant genes). Rnits compares multiple time-series expression datasets by summarizing probes into gene-level information. For all genes, it fits a series of B-splines with varying curvature and degrees of freedom. Under the null hypothesis H_0, a single model is fit for all datasets. P values from the hypothesis test are then plotted and the least complex spline parameters that result in uniformly distributed null p values are automatically chosen. Each gene is attributed a p value from 0 to 1 until all p values are uniformly distributed. While genes with p values closer to 1 have fewer changes in transcription levels between expression datasets, genes with p values closer to 0 have higher transcription levels differences between time-series expression datasets.

Protein Binding Microarrays

An enrichment score greater than 0.45 indicates high affinity binding in PBM experiments. Although the combined v9 and v11 results for the GST-D2wt control scored below 0.45, the individual v9 PBM had an E-score of 0.46 and the same binding motif was reported previously (Campbell et al., 2010). The score for each 8-mer nucleotide sequence reflects the affinity of a DNA binding domain for that sequence, with higher scores representing tighter interactions.

ChIP-Seq Data Analysis

ChIP-seq reads from 3 biological replicates were demultiplexed and then processed using FastQC (Andrew, 2010) (version 0.11.2, http://www.bioinformatics.babraham.ac.uk/projects/fastqc/) and Trimmomatic (Bolger et al., 2014). Trimming was performed by removing low quality bases and adapters using a minimum sliding window length and quality of 4 and 30, respectively, and removing reads below 36bp. Trimmed reads were mapped to the *P. falciparum* Dd2 draft genome (ftp://ftp.sanger.ac.uk/pub/pathogens/Plasmodium/falciparum/PF3K/PilotReferenceGenomes/DraftAnnotation/PfDd2/) using BWA MEM (Li, 2013), version 0.7.13-r1126, and the default parameters. SAMtools version 1.3 (Li et al., 2009) was used to remove multi-mapped reads, non-primary alignments and PCR duplicates. Peaks were called using MACS2 version 2.1.1.20160309 (Zhang et al., 2008) callpeak function and a q-value cutoff of 0.05. Only peaks that were detected in at least 2 of the 3 biological replicates were considered for further analysis; 177 trimmed peaks were further analyzed.

Anti-GFP and anti-IgG ChIP-seq libraries were compared and normalized to their respective input libraries using MACS2 for each individual replicate. Peaks within anti-IgG samples were used to filter anti-GFP libraries to remove false positives using the BEDTools suite (Quinlan and Hall, 2010) and pybedtools library (Dale et al., 2011). Peaks for each replicate were analyzed individually for technical consistency and a final list of peaks was computed by determining the overlap between biological replicates using the BEDTools *multiinter* command. These ''trimmed'' peaks represent intervals where peaks from biological replicate experiments overlapped. Only ''trimmed'' peaks present in at least 2/3 biological replicates were considered for further analysis.

Motif enrichment analysis of the trimmed peaks was done using DREME (Bailey, 2011) to identify enriched motifs between 6 and 10bp as compared to random *P. falciparum* genomic intervals of similar length. FIMO (Grant et al., 2011) was used to search 250bp upstream and downstream of peak summits for the presence of enriched sequence motifs, as found by DREME, using a p value threshold of 1e-3. Finally, TOMTOM (Gupta et al., 2007) was used to compare the de novo discovered motifs to previously in silico discovered motifs (Campbell et al., 2010); a match required a minimum overlap of 4 positions.

To build a motif heatmap (Figure 2A), the most highly enriched motif found by DREME was used to search the trimmed peak sequences. This search was done using FIMO and a threshold of 1e-3. The top-scoring motif within each sequence was assigned to its respective peak. The sequence of each peak summit was centered on these assigned motifs and ordered based on highest scoring motif according to FIMO. The position weight matrix of the aligned heatmap was obtained using the seqLogo package (Bembom, 2017). To search for enriched motifs within the peak sequences of PfBDP1 obtained from (Josling et al., 2015), we took an analogous approach, using similar thresholds and parameters.

To annotate peaks, peak summits corresponding to peaks found in at least 2/3 ChIP replicates were used to calculate the distance to target genes. Gene annotations were assigned based on their distance to the nearest downstream gene. Alignment tracks for visualization were generated using deepTools (Ramírez et al., 2014) and were visualized using the Integrated Genomics Viewer (Thorvaldsdóttir et al., 2013). Enrichment heatmaps and profile plots were generated using the deepTools computeMatrix and plotHeatmap tools. Gene Ontology (GO) enrichment analysis was done using the GO feature at PlasmoDB.org (Aurrecoechea et al., 2009).

Immunoaffinity Purification

Each immunoaffinity purification (sample and controls) was performed two independent times and only proteins that were detected in both replicates with 3 or more peptides were considered for further analysis.

The data generated was analyzed and filtered using the algorithm SAINT, which attributes a pSAINT value as a probability of interaction for each protein based on the number of spectra detected on the sample (PfAP2-I-GFP immunoaffinity purifications) versus controls immunoaffinity purifications (Choi et al., 2011).

The final list of interacting proteins was assembled by comparing the list of peptides obtained for both methods of proteolytic digestion, as described above, including only proteins with a pSAINT value (probability of interaction) equal to or above 0.9.

DATA AND SOFTWARE AVAILABILITY

ChIP-Seq Data

The accession number for the next generation sequencing data reported in this paper is NCBI Sequence Read Archive, SRA: GSE80293.

DNA Microarray Data

The accession numbers for the DNA microarray data reported in this paper is NCBI Gene Expression Omnibus, GEO: GSE77807 and GSE77810.

Protein Data

All immunoprecipitation proteomics data is available in Table S4.

Protein Binding Microarray Data

The accession number for the protein binding microarray data reported in this paper is UniPROBE: UP01415 (Hume et al., 2015). See Table S6 for position weight matrices for all AP2 domains tested by PBM.